Pulse Detonation Propulsion

S.M. Frolov
N. Semenov Institute of Chemical Physics
Moscow
RUSSIA

smfrol@chph.ras.ru

ABSTRACT

The objective of theoretical, computational and experimental studies outlined in this lecture note was to evaluate the design principles and propulsion performance of prospective air-breathing engines operating on pulse detonations of realistic hydrocarbon fuels with a realistic technique of detonation initiation via deflagration-to-detonation transition (DDT).

1.0 INTRODUCTION

Activities in the field of pulse detonation propulsion are currently focused on investigations and practical development of propulsion engines operating on propagating detonations in a pulse mode. The concept of pulse detonation engine (PDE) is attractive for both subsonic and supersonic flight with PDE as a main propulsion unit or as an afterburner in turbojet or turbofan propulsion system. In particular, PDE-based propulsion is attractive for flight Mach number up to about 3–4. Within this range of Mach number, solid rocket motors are known to be very efficient in terms of simplicity and high-speed capability, but they have a limited powered range. Turbojet and turbofan engines, due to their high specific impulse, provide longer range and heavier payloads, but at flight Mach number exceeding 2–3 they are getting too expensive. Ramjets and ducted rockets designed for flight Mach number up to 4 require solid rocket boosters to accelerate them to the ramjet take over speed, which increases the complexity and volume of a propulsion system. Combined-cycle engines, such as turborockets or turboramjets, are also very complex and expensive for similar applications.

In a PDE, detonation is initiated in a tube that serves as the combustor. The detonation wave rapidly traverses the chamber resulting in a nearly constant-volume heat addition process that produces a high pressure in the combustor and provides the thrust. The operation of PDE at high detonation-initiation frequency (about 100 Hz) can produce a near-constant thrust. In general, the near-constant volume operational cycle of PDE provides a higher thermodynamic efficiency as compared to the conventional constant-pressure (Brayton) cycle used in gas turbines and ramjets. The advantages of PDE for air-breathing propulsion are simplicity and easy scaling, reduced fuel consumption, and intrinsic capability of operation from zero approach stream velocity to high supersonic flight speeds.

In order to use propagating detonations for propulsion and realize the PDE advantages mentioned above, a number of challenging fundamental and engineering problems has yet to be solved. These problems deal basically with low-cost achievement and control of successive detonations in a propulsion device. To ensure rapid development of a detonation wave within a short cycle time, one needs to apply:

- Efficient liquid fuel injection and air supply systems to provide fast and nearly homogeneous mixing of the components in the detonation chamber;
- Low-energy source for detonation initiation to provide fast and reliable detonation onset;
- Cooling technique for rapid, preferably recuperative, heat removal from the walls of detonation chamber to ensure stable operation and avoid premature ignition of fuel–air mixture leading to detonation failure;

- Geometry of the combustion chamber to promote detonation initiation and propagation at lowest possible pressure loss and to ensure high operation frequency; and
- Control methodology that allows for adaptive, active control of the operation process to ensure optimal performance at variable flight conditions, while maintaining margin of stability.

In addition to the fundamental issues dealing with the processes in the detonation chamber, there are other issues such as:

- Efficient integration of PDE with inlets and nozzles to provide high performance;
- Durability of the propulsion system; and
- Noise and vibration.

The lecture note is organized in such a way that the reader first gets acquainted with the thermodynamic grounds for detonation-based propulsion (Section 2), followed by the principles of practical implementation of the detonation-based thermodynamic cycle in Section 3. As the main focus of this lecture is the utilization of PDE for propulsion, various performance parameters of PDEs (e.g., specific impulse, thrust, etc.) are discussed in Section 4 for the idealized PDE configuration with direct detonation initiation. The main operational constraints of PDEs are discussed in Section 5.

Section 6 is dedicated to the numerical simulation of the operation process in a more realistic PDE configuration with DDT rather than direct detonation initiation. For the numerical simulation of DDT, a coupled Flame Tracking – Particle (FTP) method combined with the look-up tables of laminar flame velocities and fuel oxidation kinetics has been developed and implemented. The method proved to be very efficient in terms of CPU requirement and has been successfully tested for several two-dimensional (2D) configurations with flame acceleration in smooth-walled channels of different length, in channels with regular obstacles, and in complex-geometry channels with orifice plates (Subsection 6.1). The results of numerical simulation of DDT in the stoichiometric propane – air mixture filling a PDE channel with regular obstacles and convergent-divergent nozzle are presented in Subsection 6.2. Thrust performances of the idealized and DDT-based propane-fueled PDEs are compared in Subsection 6.3 for the zero flight speed conditions. Section 7 presents the results of calculations of the operation process and thrust performance for the PDE under Mach 3.0 flight conditions. Finally, the operation principles and thrust performances of liquid-fueled research PDEs developed and tested at the Semenov Institute of Chemical Physics (SICP) are discussed in Section 8. The experimental data substantiate the possibility of obtaining DDT in air mixtures of practical fuels (aviation kerosene) with short run-up distances and times and with very low ignition energies.

2.0 THERMODYNAMIC GROUNDS FOR DETONATION-BASED PROPULSION

Zel'dovich [1] has shown that detonative combustion is thermodynamically more efficient than constant-volume and constant-pressure combustion. This can be seen from Fig. 1 that is the pressure (p) – specific volume (v) diagram.

Consider as an example the combustion of stoichiometric propane – air mixture:

$$C_3H_8 + 5O_2 + 18.8N_2 = 3CO_2 + 4H_2O + 18.8N_2$$

Assume that the initial thermodynamic state of the reactive mixture corresponds to point O in pressure – specific volume diagram of Fig. 1, i.e., $p = p_0, v = v_0$. The thick solid curve is the reactive mixture Hugoniot. Detonative combustion corresponds to the jump from point O to shock Hugoniot (not shown)

followed by transition to point D – Chapman–Jouguet (CJ) point – along the Reyleigh line (OD is a piece of that Reyleigh line). At point D, the entropy of combustion products is known to attain a minimum and the corresponding Poisson adiabat is tangent to the reactive Hugoniot. If one assumes that after expansion the combustion products attain the initial pressure p_0, then isentropic expansion from point D proceeds along dotted curve DD' towards point D'. In case of constant-volume combustion, the thermodynamic state of the mixture varies along vertical line OE. Further isentropic expansion proceeds along curve EE' that terminates at point E'. Finally, constant-pressure combustion results in variation of the thermodynamic state along line OG' with point G' representing the final thermodynamic state. Note that points D, E, and G' are located at the same reactive Hugoniot. Clearly, the entropy rise during detonative combustion is minimal, i.e.,

$$S_{D'} - S_O < S_{E'} - S_O < S_{G'} - S_O \tag{1}$$

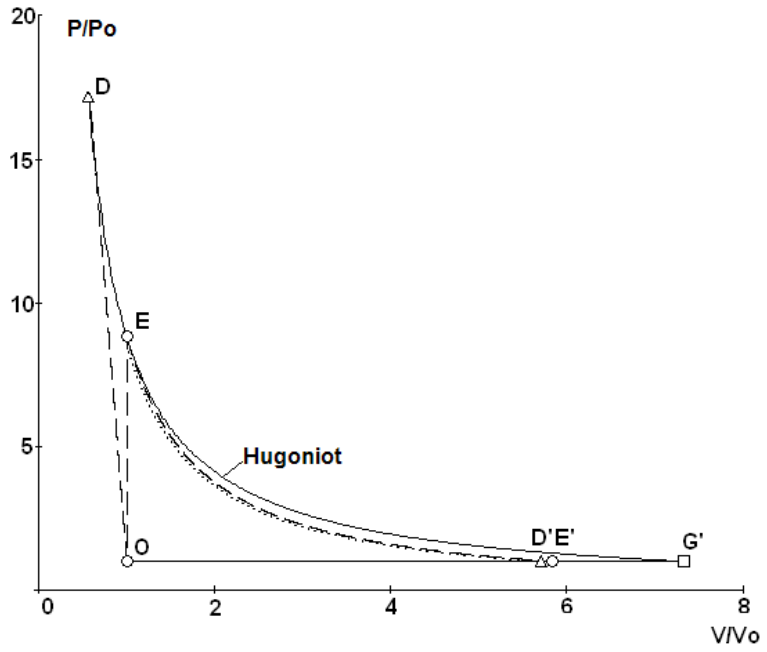

Figure 1: Thermodynamic cycles with constant-pressure, constant-volume, and detonative combustion (no precompression).

From now on, the constant-pressure, constant-volume, and detonative combustion cycles will be referred to as Brayton, Humphrey, and PDE cycles. The efficiency of thermodynamic cycles ODD'O, OEE'O, and OG'O can be readily estimated. At point O, the total specific enthalpy of the reactive mixture is $H_0 = h_0 + q$, where h_0 is the specific thermal enthalpy, and q is the heat effect of combustion. The enthalpy of the combustion products is $H = h$. The work W performed in the cycles is determined as $W = W_e - W_a = H_0 - H = h_0 - h + q$, where W_e is the expansion work and $W_a = p_0(v - v_0)$ is the work against ambient pressure. The thermal efficiency is defined as

$$\chi = \frac{W}{q} = \frac{H_0 - H}{q} \tag{2}$$

Assume that the gas obeys the ideal gas law with constant specific heats. The heat effect of combustion reaction for the stoichiometric propane – air mixture is taken equal to $q = 19760$ cal/mol (mix). Initial

temperature is taken equal to $T_0 = 300$ K. The initial mixture properties, such as specific heats at constant pressure c_{p0} and at constant volume c_{v0} are taken as $c_{p0} = 8.78$ cal/mol/K and $c_{v0} = 6.79$ cal/mol/K, so that the specific heat ratio is $\gamma_0 = c_{p0}/c_{v0} = 1.293$. The corresponding mean properties of combustion products irrespectively of the combustion mode are taken, respectively, as $c_p = 10.40$ cal/mol/K and $c_v = 8.42$ cal/mol/K, so that $\gamma = c_p/c_v = 1.235$. Figure 1 discussed above is plotted for these values of governing parameters. The reactive Hugoniot in Fig. 1 satisfies the following equation:

$$\frac{p}{p_0} = \frac{\dfrac{\gamma+1}{\gamma-1} - \dfrac{v}{v_0} + \dfrac{2\gamma}{\gamma-1}\dfrac{q}{c_p T_0}}{\dfrac{\gamma+1}{\gamma-1}\dfrac{v}{v_0} - 1}$$

As a result of constant-pressure combustion, the temperature, pressure, and specific volume of combustion products at point G' in Fig. 1 are $T_{G'} = T_0 + q/c_p = 2199$ K, $p_{G'} = p_0$, and $v_{G'} = 7.33 v_0$, giving $H_{G'} = c_{p0}T_0 + c_p(T_{G'} - T_0) = 22390$ cal/mol. Combustion at constant ambient pressure (without mixture precompression) results in zero thermodynamic efficiency of Brayton cycle, as $H_{G'} = H_0$, i.e.,

$$\chi_{p=const} = 0 \tag{3}$$

Constant-volume combustion (point E in Fig. 1) results in temperature $T_E = T_0 + q/c_v = 2647$ K, pressure $p_E = p_0 T_E/T_0 = 8.82 p_0$, and specific volume $v_E = v_0$. Isentropic expansion of combustion products from p_E to p_0 results in temperature drop from T_E to $T_{E'} = T_E(p_E/p_0)^{-(\gamma-1)/\gamma} \approx 1749$ K, giving $H_{E'} = c_{p0}T_0 + c_p(T_{E'} - T_0) = 17700$ cal/mol (point E' in Fig. 1). Substituting the value of $H = H_{E'}$ into Eq. (2) one obtains the efficiency of the Humphrey cycle:

$$\chi_{V=const} = \frac{H_0 - H_{E'}}{q} \approx 0.238 \tag{4}$$

At point D in Fig. 1, pressure, temperature, and specific volume of detonation products are estimated as

$$p_D = p_0[1 + \gamma(M_{CJ}^2 - 1)/(\gamma+1)] \approx 17.178 p_0$$

$$T_D = T_0\left(\frac{p_D}{M_{CJ} p_0}\right)^2 \approx 2924\,\text{K}$$

$$v_D = v_0\left(\frac{T_D}{T_0}\frac{p_0}{p_D}\right) \approx 0.567 v_0$$

where

$$M_{CJ} = \sqrt{1 + (\gamma+1)q/2c_pT_0} + \sqrt{(\gamma+1)q/2c_pT_0}$$

is the Mach number of the CJ detonation wave (detonation velocity is 1804 m/s). Isentropic expansion of detonation products from p_D to p_0 results in temperature drop from T_D to $T_{D'} = T_D(p_D/p_0)^{-(\gamma-1)/\gamma} =$

1702 K, giving $H_{D'} = c_{p0}T_0 + c_p(T_{D'} - T_0) = 17210$ cal/mol. Substituting the value $H = H_{D'}$ into Eq. (2) one obtains the efficiency of the PDE cycle with detonative combustion:

$$\chi_{\text{Detonation}} = \frac{H_0 - H_{D'}}{q} = 0.262 \tag{5}$$

Comparing Eqs. (3), (4), and (5) one comes to the following relation between the thermal efficiencies of Brayton, Humphrey, and PDE cycles without initial mixture precompression:

$$\chi_{\text{Detonation}} > \chi_{V=const} > \chi_{p=const} \tag{6}$$

As $T_{D'} \approx 1702$ K, $T_{E'} \approx 1749$ K, and $T_{G'} = 2199$ K, the relationship (1) between entropy change in processes ODD', OEE', and OG' is now substantiated quantitatively.

Mixture precompression results in the pressure – specific volume diagram of the type shown in Fig. 2. Mixture precompression can be attained by using a mechanical compressor and/or by decelerating the flow in a combustor (ram compression). In the latter case, the relationships between the vehicle flight Mach number M_∞ and ram compression ratio $\pi = \pi_R$ is

$$\pi_R = \left(1 + \frac{\gamma_0 - 1}{2} M_\infty^2\right)^{\frac{\gamma_0}{\gamma_0 - 1}}, \qquad M_\infty = \sqrt{\frac{2}{\gamma_0 - 1}\left(\pi_R^{\frac{\gamma_0 - 1}{\gamma_0}} - 1\right)}$$

if ideal isentropic compression (without shocks) to stagnation parameters is assumed. Analysis shows that in terms of the gain in ideal thermal efficiency, the PDE cycle in an engine with purely ram compression is favorable at flight Mach numbers $0 < M_\infty < 3$–4, being most favorable at subsonic, transonic, and moderate supersonic flight speeds. At $M_\infty > 3 - 4$, the difference in ideal thermal efficiencies of the cycles becomes less pronounced.

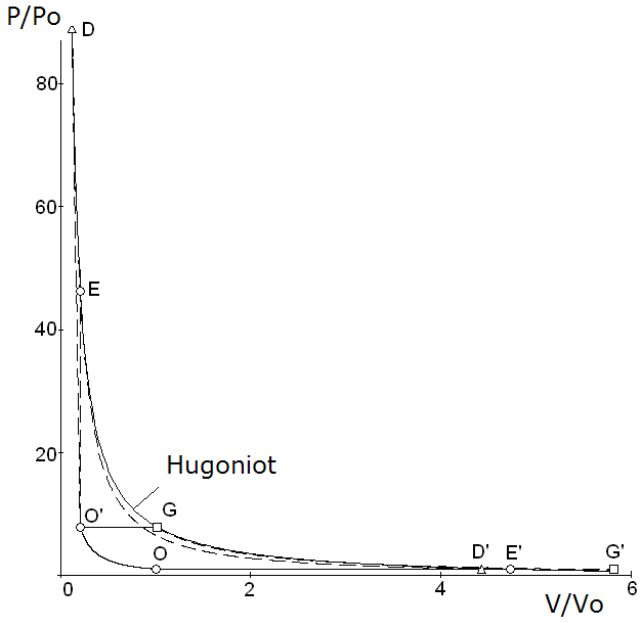

Figure 2: Thermodynamic cycles with constant-pressure, constant-volume, and detonative combustion (with precompression).

To show the effect of presompression on the thermal efficiency, assume ideal isentropic compression of initial mixture from state O to state O' with ram compression ratio $\pi_R = 7.82$ corresponding to flight Mach number 2.0. The thermodynamic parameters in state O' are: temperature $T_{O'} = T_0 \pi_R^{(\gamma-1)/\gamma} \approx 478\,\mathrm{K}$, pressure $p_{O'} = \pi_R p_0 = 7.82\,p_0$, specific volume $v_{O'} = v_0\left(p_0 T_{O'} / p_{O'} T_0\right) \approx 0.204 v_0$, and the specific enthalpy is

$$H_{O'} = c_{p0} T_0 \pi_R^{(\gamma-1)/\gamma} + q \approx 4198 \text{ cal/mol} + q$$

Further energy release due to detonative, constant-volume, or constant-pressure combustion results in transition from state O' to state D, E, or G, respectively, located on the reactive Hugoniot:

$$\frac{p}{p_{O'}} = \frac{\dfrac{\gamma+1}{\gamma-1} - \dfrac{v}{v_{O'}} + \dfrac{2\gamma}{\gamma-1}\dfrac{q}{c_p T_{O'}}}{\dfrac{\gamma+1}{\gamma-1}\dfrac{v}{v_{O'}} - 1}$$

which is different from that shown in Fig. 1 as it contains parameters at state O' rather than at state O. Isentropic expansion of combustion products to the ambient pressure p_0 results in new final states D', E', or G', depending on the combustion mode.

At constant-pressure combustion (Brayton cycle OO'GG'O), the enthalpy of the combustion products at point G is $H_G = H_{O'}$ resulting in temperature $T_G = T_{O'} + q/c_p \approx 2378\,\mathrm{K}$, pressure $p_G = 7.82\,p_0$, and specific volume $v_G = v_0\left(p_0 T_G / p_G T_0\right) \approx 1.013 v_0$. Isentropic expansion of combustion products from p_G to p_0 results in temperature drop from T_G to $T_{G'} = 1608\,\mathrm{K}$, increase in the specific volume from v_G to $v_{G'} = v_0\left(p_0 T_{G'} / p_{G'} T_0\right) \approx 5.818 v_0$, giving $H_{G'} = 15950$ cal/mol. The efficiency of cycle OO'GG'O is then equal to

$$\chi_{p=const} = \frac{H_0 - H_{G'}}{q} = \frac{c_{p0}T_0 + q - H_{G'}}{q} \approx 0.326$$

Constant-volume combustion (Humphrey cycle OO'EE'O) results in temperature $T_E = T_{O'} + q/c_v = 2825\,\mathrm{K}$, specific volume $v_E = v_{O'} = 0.204v_0$, and pressure $p_E = p_{O'}(T_E/T_{O'}) \approx 46.2\,p_0$. Isentropic expansion of combustion products from p_E to p_0 results in temperature drop from T_E to $T_{E'} = T_E(p_E/p_0)^{-(\gamma-1)/\gamma} \approx 1362$ K, increase in the specific volume from v_E to $v_{E'} = v_0(T_{E'}/T_0) \approx 4.726v_0$ and $H_{E'} = c_p T_{E'} \approx 13390$ cal/mol. Thus, the efficiency of cycle OO'EE'O is:

$$\chi_{V=const} = \frac{H_0 - H_{E'}}{q} \approx 0.456$$

At point D, pressure, temperature, and specific volume of detonation products are estimated as

$$p_D = p_{O'}[1 + \gamma(M_{CJ}^2 - 1)/(\gamma + 1)] \approx 88.675\,p_0$$

$$T_D = T_{O'}\left(\frac{p_D}{M_{CJ}\,p_{O'}}\right)^2 \approx 3119\,\mathrm{K}$$

$$v_D = v_0\left(\frac{T_D}{T_0}\frac{p_0}{p_D}\right) \approx 0.117v_0$$

where the Mach number of the CJ detonation wave is equal to

$$M_{CJ} = \sqrt{1 + (\gamma+1)q/2c_pT_{O'}} + \sqrt{(\gamma+1)q/2c_pT_{O'}} \approx 4.44$$

Isentropic expansion of detonation products from p_D to p_0 results in temperature drop from T_D to $T_{D'} = T_D(p_D/p_0)^{-(\gamma-1)/\gamma} = 1328$ K and increasing specific volume from v_D to $v_{D'} = v_0(T_{D'}/T_0) \approx 4.426v_0$, giving $H_{D'} = c_p T_{D'} = 13040$ cal/mol. The efficiency of PDE cycle OO'DD'O:

$$\chi_{Detonation} = \frac{H_0 - H_{D'}}{q} = 0.473$$

Using the same procedure, one can estimate cycle efficiencies for various values of precompression ratio π_R. Figure 3 shows the calculated dependencies of $\chi_{p=const}$ (Brayton cycle), $\chi_{V=const}$ (Humphrey cycle), and $\chi_{Detonation}$ (PDE cycle) depending on the compression ratio π.

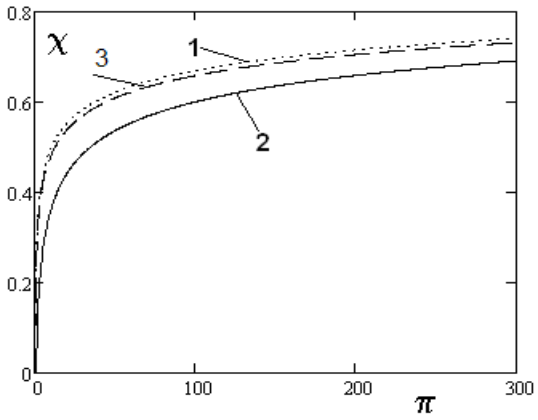

Figure 3: Predicted thermodynamic efficiency of PDE (*1*), Brayton (*2*), and Humphry (*3*) cycles depending on the precompression ratio π.

Thus, precompression of the reactive mixture increases the efficiency of all cycles under consideration, however leaving valid the relationships (1) and (6). Calculations of comparative cycle efficiencies with realistic thermodynamics gives qualitatively similar results to those discussed above [2–4].

3.0 PDE CYCLE

The PDE cycle applies a concept of fuel combustion in repeatedly generated detonation waves traversing the combustion chamber [5–10]. The thermal efficiency of the ramjet cycle with such a repeated (pulsed) process will evidently depend on the frequency of generation of detonation waves. This device, referred to as a PDE, is the primary focus of this lecture.

According to current understanding, the PDE comprises (Fig. 4):

- Air intake ensuring continuous inflow and compression of air from the ambient atmospheric pressure to a certain stagnation pressure;
- Receiver, where the air passing from the air intake is divided into two streams: one to the detonation chamber and the other to the annular bypass channel;
- Valve-distribution system, which forces air to pass from the receiver either to the detonation chamber or to the bypass channel in a given time sequence;
- Detonation chamber consisting of a tube with fuel injector and detonation initiator at the entrance;
- Supersonic nozzle; and
- Fuel tanks and systems of fuel injection.

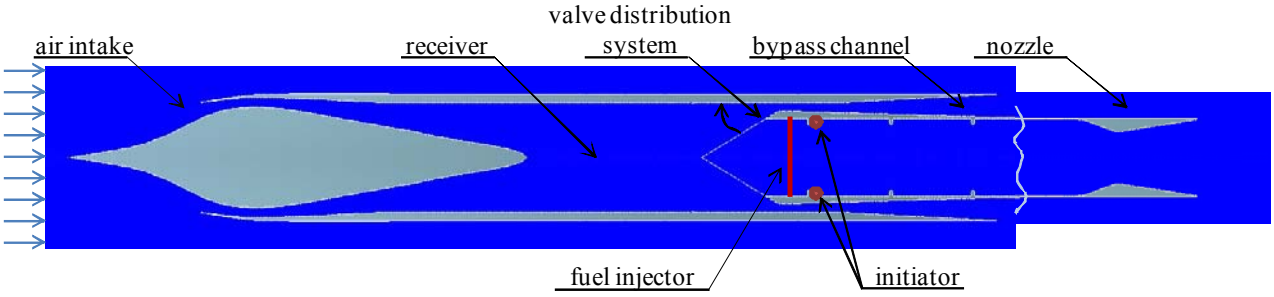

Figure 4: Pulsed detonation engine with supersonic air intake, bypass channel, mechanical valve, and nozzle.

The operation cycle of a PDE includes the following phases:

- Injection of fuel into the detonation chamber and mixing of fuel with incoming air;
- Valve closing and mixture ignition;
- DDT and mixture burnout in a propagating detonation wave; and
- Expansion of detonation products through a supersonic nozzle.

Subsequent valve opening and fuel injection into the detonation chamber starts the new operation cycle. The mechanical valve is used to prevent detonations or shocks from moving outward through the air intake and to ensure a controlled inward flow rate of fresh air. Various valveless PDE configurations are also considered [9]. To reduce thrust pulsations and noise, multitube configurations of PDE are proposed that imply the use of phase shift between processes in different tubes.

4.0 SPECIFIC IMPULSE OF IDEALIZED PDE

The simplest (idealized) PDE configuration with direct detonation initiation is shown in Fig. 5. We consider a planar 2D configuration with a straight smooth-walled PDE channel of height (H = 52 mm) and length (L = 3 m) filled with the stoichiometric propane – air mixture at normal initial conditions ($p_0 = 1$ atm, $T_0 = 293$ K). The detonation is initiated at the closed end of the PDE channel by making a provision for the high-pressure (40 atm) initiation section with the length $l = H$ filled with hot combustion products of the stoichiometric propane – air mixture at temperature 3300 K. To facilitate detonation initiation, the initial velocity of the products was taken equal to 2000 m/s. The calculations are performed using a CFD code solving Reynolds Averaged Navier – Stokes (RANS) equations by the control-volume approach with 5-step overall propane oxidation chemistry implemented through the Particle method [11].

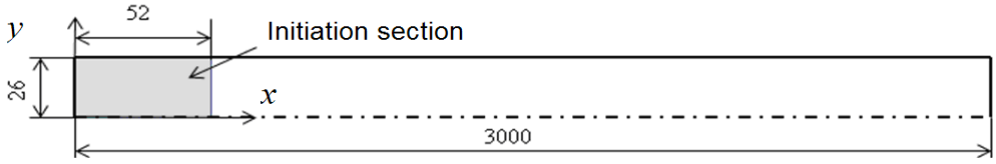

Figure 5: Schematic of an idealized PDE with a section for direct detonation initiation.

For the PDE channel of Fig. 5,the thrust performance parameters can be estimated using the following equations:

- Specific (per unit area) thrust P :

$$P(t) = \frac{1}{F_e}\int_{F_e}[\rho_e(t,y)U_e^2(t,y) + p_e(t,y) - p_0]dF \tag{7}$$

- Impulse per unit area I:

$$I = \int_0^{t_c} P(t)dt \tag{8}$$

- Specific fuel-based impulse I_{sp}:

$$I_{sp} = F_e\frac{I}{m_f g} \tag{9}$$

In Eqs. (7)–(9), F is the cross section area of the PDE channel, ρ, U, and p are the gas density, velocity, and pressure, respectively, index e relates to the PDE channel outlet, t_c is the PDE channel evacuation time (the time taken for $P(t)$ to attain the maximum value), m_f is the fuel mass in the PDE channel, and g is the acceleration of gravity.

Obviously, the value of the specific impulse should be close to the value obtained by direct integration of the pressure over the PDE thrust wall. Some small differences can arise due to momentum and energy losses at the smooth walls of the PDE channel. Defining the force acting at the unit area of the thrust wall P_T and impulse per unit area I_T as

$$P_T(t) = \frac{1}{F_T}\int_{F_T}[p_T(t) - p_0]dF \tag{10}$$

and

$$I_T = \int_0^{t_c} P_T(t)dt \tag{11}$$

where index T relates to the thrust wall, one obtains

$$I_{sp,T} = F_T\frac{I_T}{m_f g} \tag{12}$$

The curve in Fig. 6 shows the specific thrust history at the outlet of the PDE channel for this case. For the sake of convenience, Fig. 6a shows the specific thrust history for the early stage of the exhaust process ($t < 12$ ms) and Fig. 6b for its late stage ($9 < t < 50$ ms). The area under the curve in Fig. 6, is approximately equal to $I \approx 5040 \pm 100$ Pa·s (the estimated calculation error of I is 2%). Taking into account that $m_f \approx 0.00547$ kg/m, $F_e = 0.026$ m^2/m, and $g = 9.8$ m/s^2 one comes to the following value of the specific impulse I_{sp} of Eq. (9):

$$I_{sp} = F_e\frac{I}{m_f g} \approx 0.026\frac{5040}{0.00547 \cdot 9.8} = 2440 \pm 50 \text{ s} \tag{13}$$

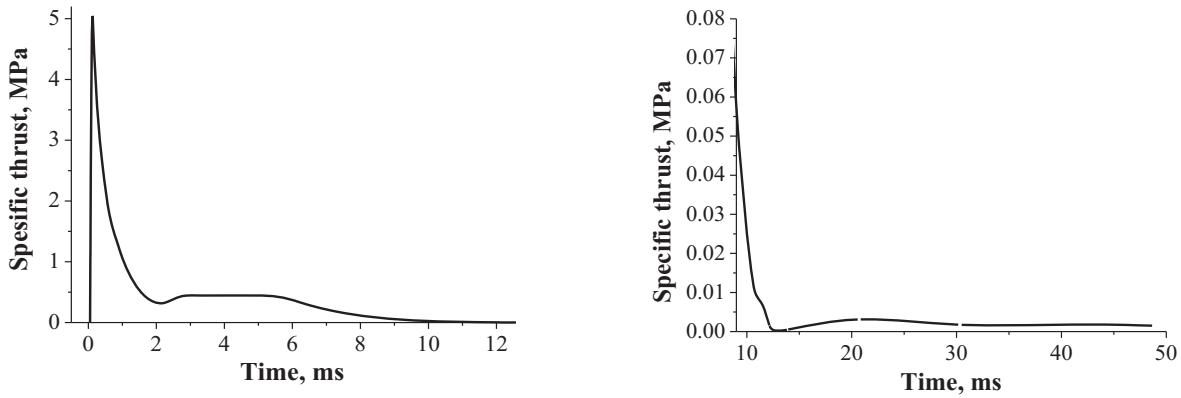

(a) (b)

Figure 6: Time histories of the specific (per unit area) thrust calculated based on the exhaust flow parameters at the PDE channel exit at direct detonation initiation in a straight smooth-walled channel: (a) $t < 12$ ms, (b) $9 < t < 50$ ms.

As expected, application of Eqs. (10)–(12) shows that $I_{sp,T} \approx I_{sp}$, i.e., for the idealized PDE of Fig. 5 skin friction and heat losses can be neglected.

It is instructive to compare the present results of numerical simulation in the straight smooth-walled PDE channel with the results available in the literature. According to one-dimensional (1D) analysis [12, 13], the impulse per unit area I is equal to

$$I \approx K(p_{TZ} - p_0)t_{CJ} \tag{14}$$

where $t_{CJ} = L / D_{CJ}$ is the residence time of the detonation in the PDE channel, p_{TZ} is the Taylor–Zel'dovich "detonation kernel" pressure, and K is the coefficient which is somewhat different in various studies due to details of direct detonation initiation, channel geometry, etc.: $K = 4.65$ in [13], 4.85 in [14], and 5.15 in [12]. The value of p_{TZ} can be calculated as [12]:

$$p_{TZ} = p_{CJ}\left(\frac{\gamma+1}{2\gamma}\right)^{2\gamma/(\gamma-1)}$$

where p_{CJ} is the Chapman–Jouguet pressure and γ is the ratio of specific heats in the detonation products. Detailed thermodynamic calculations for the stoichiometric propane – air mixture at normal initial conditions give p_{CJ} =1.827 MPa and $\gamma \approx 1.166$, therefore $p_{TZ} \approx 0.65$ MPa. The "ideal" residence time in the example under consideration is $t_{CJ} \approx 3/1804 \approx 1.66$ ms. Substituting these values to Eq. (14) gives

$$I \approx 4250 - 4700 \text{ Pa} \cdot \text{s}$$

The corresponding value of the specific impulse is

$$I_{sp} \approx 2010 - 2230 \text{ s}$$

These values are less than those obtained in the present 2D calculations (5040 ± 100 Pa·s and 2440 ± 50 s, respectively). The excess impulse in the present calculations (about 13% in average) can be explained by the contribution of the detonation initiator [13]. According to [13], depending on the tube length and initiator energy, the initiator contribution to the impulse can be as large as 17% to 27%.

Note that the self-sustained Chapman–Jouguet detonation in our computational example propagates with the constant velocity close to 1900 m/s. This velocity corresponds to the thermodynamically equilibrium value calculated based on the truncated composition of reaction products (only CO_2, H_2O, CO, H_2, C_3H_8, and O_2 species are considered in the 5-step reaction scheme of propane oxidation). Note that this value is about 5% higher than the thermodynamic detonation velocity $D_{CJ} \approx 1804$ m/s calculated based on the extended composition of reaction products [15].

Thus, the fuel-based specific impulse of PDE in the configuration of Fig. 5 predicted for the conditions of zero flight speed exceeds considerably the maximum attainable fuel-based specific impulse of a ramjet, which vanishes at zero flight-speed conditions and attains the maximum value of about 1600–1800 s at optimal supersonic flight conditions.

5.0 OPERATIONAL CONSTRAINTS

It is instructive to indicate the range of operation conditions for the PDE assuming that it is designed for producing thrust for a flying vehicle.

The basic requirement to the PDE fuel is that it should readily detonate with low sensitivity to initial conditions in terms of pressure, temperature, and mixture composition.

Another requirement to the PDE fuel, which contradicts the above requirement, is avoiding surface ignition of explosive mixture before or after triggering the initiator, or uncontrolled autoignition of the mixture due to mixing with residual combustion products. Premature ignition is expected to arise near the hot walls of the detonation chamber (at temperatures exceeding ~ 800 K), providing that the cycle duration is longer than the autoignition delay. In view of it, the PDE fuel should exhibit high resistance to ignition by a hot surface. A particular issue is avoiding premature ignition in the vicinity of the initiator. It is expected that the surfaces located near the initiator and the initiator itself can get very hot during operation, and the abnormal combustion can produce thermal damage in a very short time.

For propulsion applications, the PDE fuel is preferably a liquid hydrocarbon (or other liquid compound) due to high energy density. The requirement of fast mixing of fuel with incoming air implies that the PDE fuel should exhibit high vapor pressure at operation conditions. One of possible solutions is recuperative fuel preheating or prevaporization. The presence in the PDE fuel of nonvolatile hydrocarbons and additives containing metals and polymeric compounds can promote premature ignition due to their deposit-forming tendency. The deposits are known to produce the thermal isolation effect increasing the wall temperature.

The other very important issue is detonation initiation. On the one hand, the energy requirements for direct detonation initiation in an air-breathing PDE operating on standard hydrocarbon fuels are too high. Thus, for direct detonation initiation of the stoichiometric propane – air mixture one needs tens of grams of high explosive (e.g., TNT) per cycle which is absolutely unfeasible for a multipulse PDE operation. On the other hand, DDT in a gaseous propane–air mixture requires very long tubes: no less than 260 tube diameters for a straight smooth tube [16] and more than 60 tube diameters for a straight tube with turbulence promoters in the form of regular obstacles [17, 18]. Therefore there is a need in the development of efficient means for reducing the DDT run-up distance and time for gas- and liquid-fueled air-breathing PDE applications. By other words, one has to ensure fast DDT in a PDE tube at the lowest

possible ignition energy, at the shortest distance, with the lowest pressure loss. In view of it, all realistic estimates of PDE performances have to be based on the consideration of fast DDT rather than direct detonation initiation in the PDE tube.

The existence of detonability limits dictates the constraints on combustor diameter and mass flow rate. The length of the combustion chamber determines the combustor volume and overall operating frequency because of the individual processes that must occur for each cycle. The operating frequency f of a given engine is defined as $1/t_c$, where cycle duration t_c is composed, in general, of five characteristic time intervals: filling Δt_{fl}, purging Δt_{pr}, detonation initiation Δt_{in}, detonation traversing the combustor Δt_{tr}, and exhaust Δt_{ex}, i.e.,

$$t_c = \Delta t_{fl} + \Delta t_{pr} + \Delta t_{in} + \Delta t_{tr} + \Delta t_{ex}$$

The dynamic filling and exhaust/purging processes tend to be the longest duration and can be shortened by operating at higher dynamic pressures, but with some upper limit due to filling losses. The length of the combustor and the filling velocity determine the fill time, Δt_{fl}, since the mass flow into the combustor has to traverse the derived combustor length. Since the length, flight dynamic pressure, and operating frequency of a combustor are directly coupled, an optimum will likely exist where performance will be maximized. Practical values of operation frequency are near 100 Hz, but this frequency limit could be overcome if multiple injection locations are utilized.

In addition to the fuel detonability requirements mentioned above, a set of vehicle design requirements (low pressure loss, low weight, size constraints, etc.) should be met. Clearly, some of the requirements appear to be quite contradictory, and a sort of compromise must usually be achieved.

6.0 SIMULATION OF OPERATION PROCESS IN NONIDEALIZED PDE

More realistic estimates of PDE performances, as compared to those obtained with the presumption of direct detonation initiation require the availability of a computationally efficient algorithm for multidimensional numerical simulation of DDT in gas- and liquid-fueled air-breathing PDE. Recently, we have developed such an algorithm which is based on the coupled FTP method [11]. The method allows simulating both frontal and volumetric combustion in a compressible flow, in particular, flame acceleration in a channel of complex geometry followed by preflame autoignition and transition to a detonation.

The coupled FTP method has been implemented into the standard CFD code solving the RANS equations by the control-volume technique. The method has been thoroughly validated against experimental data on flame acceleration in smooth-walled and obstructed channels with one closed and one open end. Such channel configurations are directly relevant to PDE applications.

6.1 FTP Method Validation

Smooth-Walled Channel

The FTP method has been first used for calculating flame propagation in straight rectangular 40x40 mm smooth-walled channels 2.6, 3.5, 5.1, and 6.1 m long with one closed and one open end filled with the stoichiometric propane – air mixture at normal initial conditions as used in experiments [19].

Figure 7 compares the results of calculations with the experiments in terms of the time histories of the distance traveled by the flame. Solid curves correspond to the predicted results whereas the dashed curves correspond to the measurements.

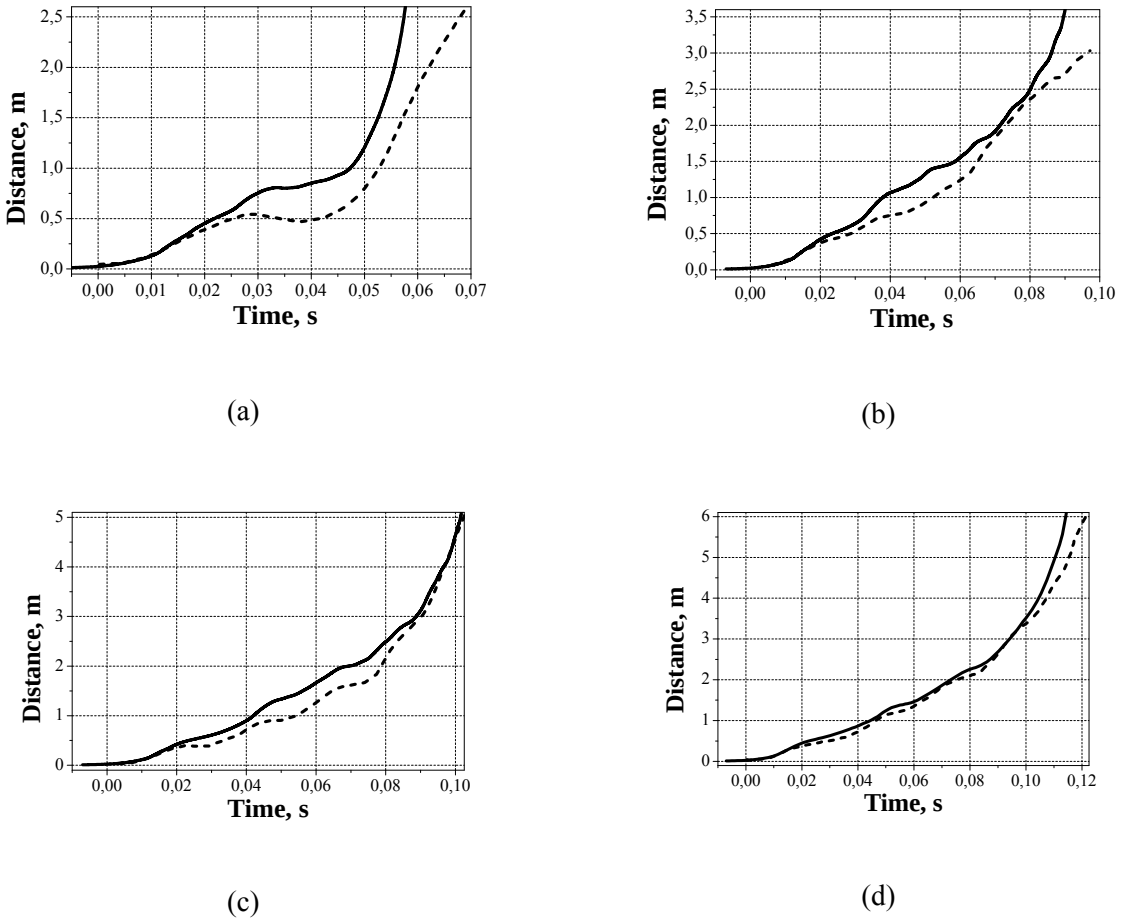

Figure 7: Comparison between predicted (solid curves) and measured [19] (dashed curves) distances traveled by the flame vs. time in 40 x 40 mm straight channels of different lengths filled with the stoichiometric propane–air mixture: (a) channel length 2.6 m, (b) 3.6 m, (c) 5.1 m, and (d) 6.1 m.

The walls of the channel were assumed isothermal ($T_w = 293$ K). At the open end, a constant-pressure ($p_0 = 1$ atm) boundary condition was applied. The stoichiometric propane – air mixture was assumed initially quiescent at $T_0 = 293$ K and $p_0 = 1$ atm.

The initial flame kernel was taken as a circle 1 mm in radius with the center located at 1 cm from the closed end-wall at the symmetry plane (similar to experimental ignition conditions). The internal energy of the gas in the kernel (ignition energy) was on the order of 1 mJ.

The turbulent flame velocity u_t was modeled by the Shchelkin formula:

$$u_t \approx u_n \sqrt{1 + u'^2 / u_n^2} \tag{15}$$

where u' is the local instantaneous turbulence intensity, related to the turbulent kinetic energy or to pulsating velocity correlations, and u_n is the local instantaneous laminar burning velocity. Turbulence was modeled by the standard k–ε model. The laminar burning velocity u_n was linearly interpolated using the data of extended look-up tables.

The computational grid was uniform with square cells 2 x 2 mm. On the subgrid level, the flame front in a computational cell was normally represented by no less than 15 segments.

As seen from Fig. 7, the predicted flame front trajectories agree satisfactory with the measurements despite the 2D representation of essentially three-dimensional (3D) phenomena in the experiments. It is worth noting that the numerical simulation is capable of adequate predicting the effect of various pressure waves on flame motion which is obvious from simultaneous appearance of crests on the curves.

Differentiation of solid curves shown in Fig. 7 allows obtaining the local instantaneous visible velocities of flame propagation. As an example, Fig. 8 shows the time history of visible flame velocity in the tube 6.1 m long. Towards the end of the tube, the visible flame velocity is seen to increase up to nearly 450 m/s. Flame acceleration is not monotonous. The periodic drops and humps in the visible flame velocity are caused by flame interactions with compression/rarefaction waves reflected from the open and closed ends of the channel. Such interactions result not only in flame deceleration/acceleration, but also in the variation of flame shape. Figure 9 shows the shapes of the flame at different stages of its propagation in the 6.1-meter tube. Clearly, flame – pressure wave interactions result in drastic changes of the mean flame shape. Very similar qualitative and quantitative findings are reported in [19].

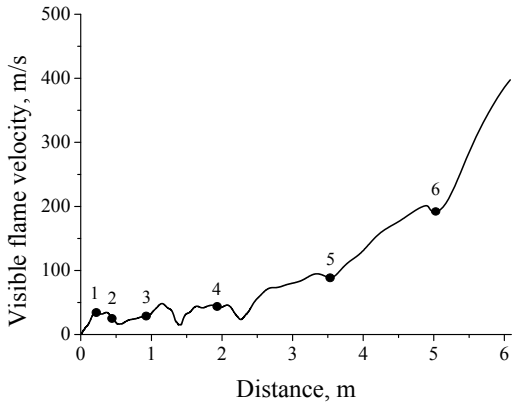

Figure 8: Predicted flame propagation velocity in the 6.1-meter tube. Black dots denote locations with different flame shapes, shown in Fig. 5.

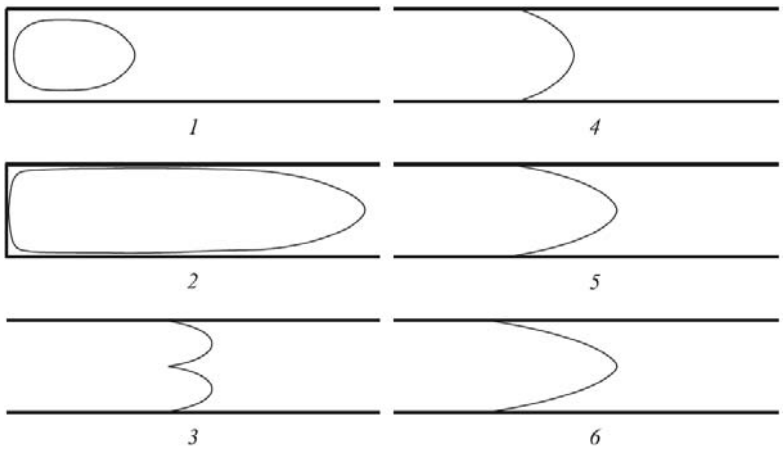

Figure 9: Snapshots of mean flame shapes at different locations in the 6.1-meter tube, shown by black dots in Fig. 8.

It is worth noting that the FTP method avoids numerical smearing of the flame front: the combustion products are separated from the fresh mixture through a single computational cell in which flame segments are located.

Channel with Regular Obstacles

As an example of code performance for accelerating flames in obstructed tubes, let us consider the results of three test cases with flame acceleration in the straight cylindrical tube of internal diameter $D = 152$ mm and length $L = 3.1$ m with one open end and regular obstacles in the form of orifice plates with blockage ratio 0.43, 0.6, and 0.75 filled with the stoichiometric propane – air mixture at normal initial conditions as used in experiments [20]. The blockage ratio of orifice plates was defined as BR = $1-(d/D)^2$, where d is the orifice diameter. In the experiments, the mixture was initially quiescent and spark ignition took place at the closed end of the tube.

The geometries of the tubes were represented by axisymmetrical geometries in the calculations. The walls of the tube were assumed isothermal ($T_w = 293$ K). At the open end, a constant-pressure ($p_0 = 1$ atm) boundary condition was applied. The use of nonreflecting boundary conditions at the walls of a buffer volume of a larger cross section attached to the open end of the tube did not affect significantly the results of calculations leading however to increasing CPU time.

The stoichiometric propane – air mixture was assumed initially quiescent at $T_0 = 293$ K and $p_0 =$ 1 atm. The initial flame kernel was taken as a circle 1 mm in radius with the center located at 1 cm from the closed end-wall at the symmetry plane. The ignition energy was on the order of 1 mJ. The turbulent flame velocity was modeled by the Shchelkin formula (Eq. (15)). Turbulence was modeled by the standard k–ε model. The computational grids were structured with the mean cell size of 2 mm. The flame front in a computational cell was normally represented by no less than 15 segments.

Figure 10 compares predicted visible flame velocities (curves) with experimental data [20] (symbols) depending on the distance traveled by the flame for the three different values of BR. In all cases, the distance between neighboring orifice plates (pitch S) was equal to tube diameter $S = D$.

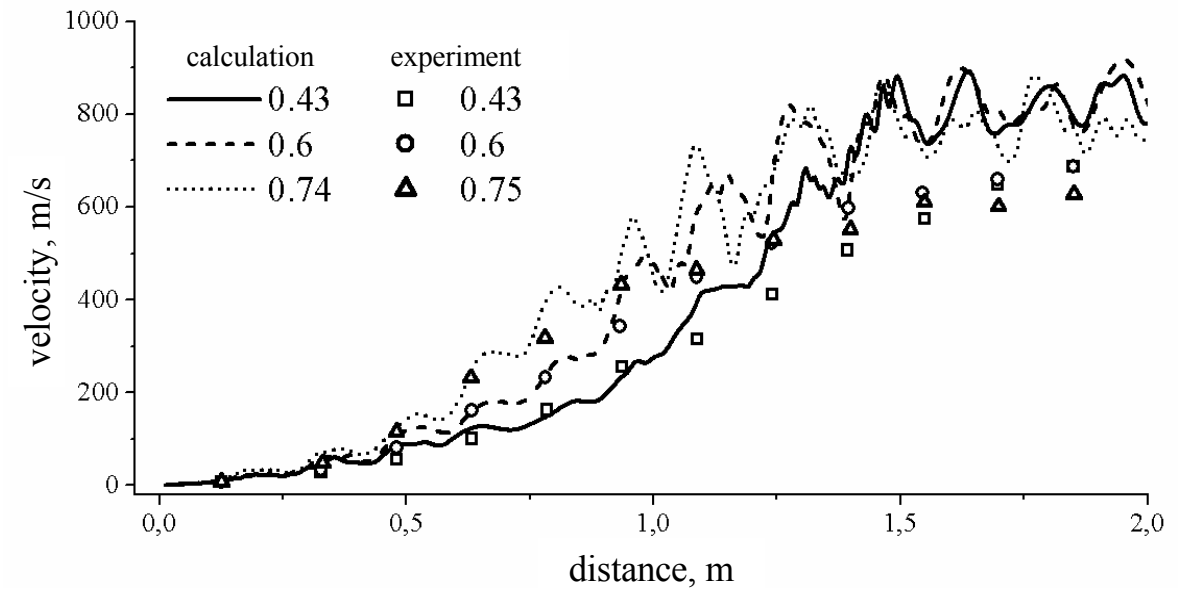

Figure 10: Predicted (curves) and measured (symbols [20]) visible flame velocities vs. distance in tubes of $D = 152$ mm with regular orifice plates (BR = 0.43, 0.6, and 0.75, pitch $S = D$). Stoichometric propane – air mixture at $T_0 = 293$ K and $p_0 = 1$ atm.

In general, satisfactory agreement between predicted and measured values of flame velocity is worth mentioning. Very good agreement is attained at the initial phase of flame acceleration, where its velocity is less than 300–400 m/s. The flame accelerates to about 800–900 m/s, i.e., to the velocity close to the sound speed in the combustion products (about 890 m/s). Initially, the flame accelerates faster in the tube with orifice plates of larger BR. This is probably caused by a higher level of turbulence generated by such obstacles. However further flame acceleration results in growing momentum losses and the efficiency of orifice plates with high BR in terms of flame acceleration decreases.

Complex Geometry Duct

Code performance was also validated for stoichiometric methane – air flame acceleration in the complex-geometry duct shown in Fig. 11 with a prechamber 326 mm long, expansion volume 280 mm long, and a tube 2470 mm long with orifice plates and perforated partitions. In the experiments performed at SICP, the mixture was ignited by a spark plug at the left (closed) end of the prechamber. After traversing the prechamber, the accelerating turbulent flame entered the expansion volume through a nozzle 16 mm in diameter. In the expansion volume, flame further accelerated when passed through the perforated partition with 12 orifices, each 14 mm in diameter. Thereafter the flame transitioned to the 70-mm diameter tube with an array of regular obstacles in the form of orifice plates with the blockage ratio BR = 0.5 and spacing equal to tube diameter (70 mm). The far (right) end of the tube was open to the atmosphere.

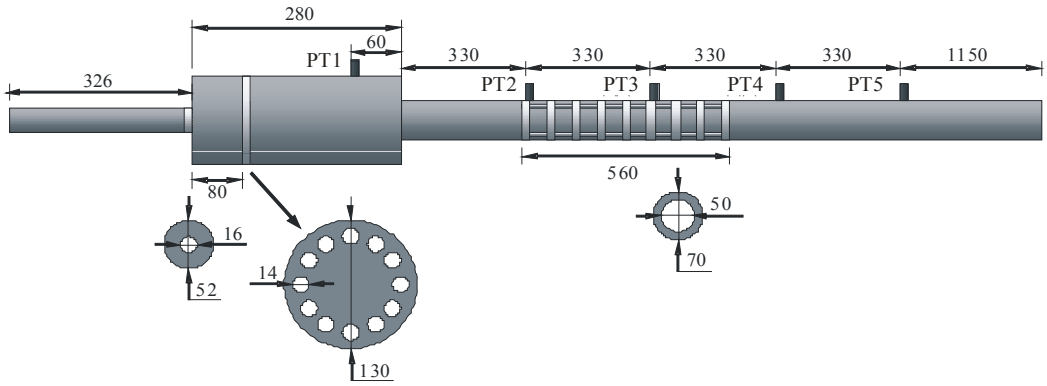

Figure 11: Schematic of experimental setup (PT stands for pressure transducer). Dimensions are in millimeters.

In the calculations, the duct of Fig. 11 was represented by the axisymmetrical geometry. The stoichiometric mehane – air mixture was assumed initially quiescent at $T_0 = 293$ K and $p_0 =$ 1 atm. All settings were the same as in the previous validation examples.

Figure 12 compares the predicted and measured mean shock wave velocities at three measuring segments PT2–PT3, PT3–PT4, and PT4–PT5. Figure 13 compares predicted and measured pressure histories at locations of pressure transducers PT1 to PT5. Taking into account the complexity of setup geometry, the results of calculations can be treated as very encouraging.

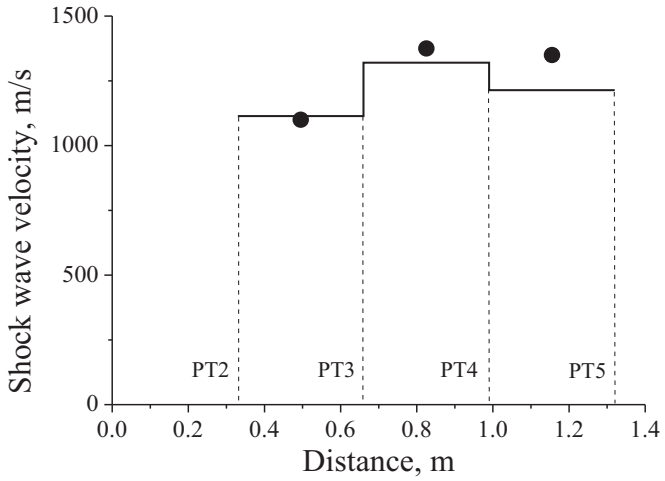

Figure 12: Comparison of predicted (line) and measured (circles) shock wave velocities in the setup of Fig. 11. Height of circles corresponds to the error of velocity measurement. Distance is measured from the outlet of the extension volume.

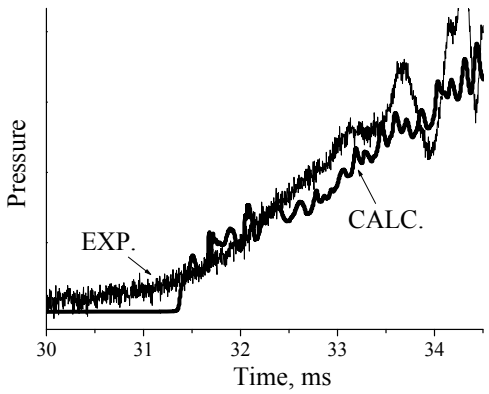

PT1

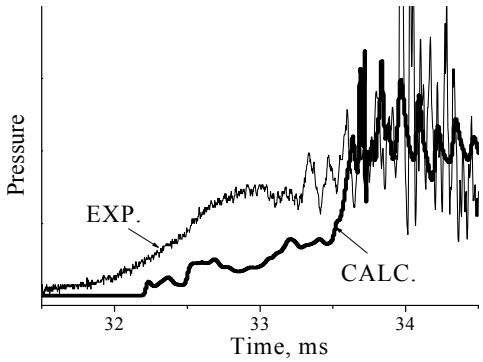

PT2

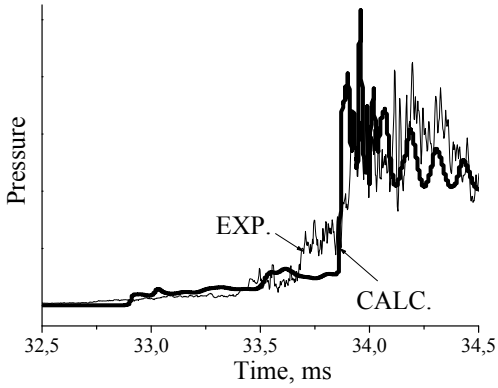

PT3

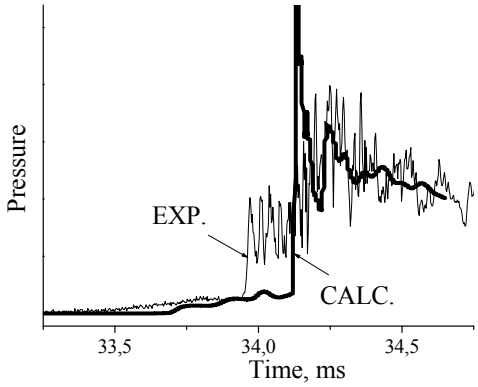

PT4

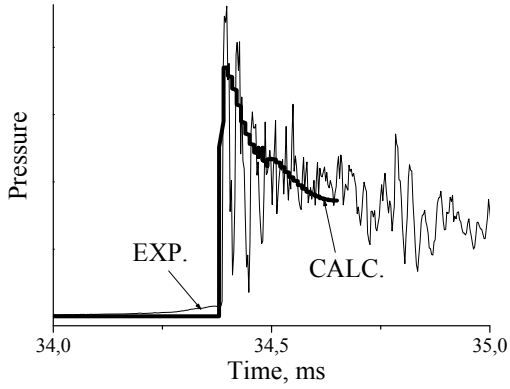

PT5

Figure 13: Comparison of predicted and measured pressure histories at pressure transducers PT1 to PT5 in the setup of Fig. 11. Time is measured from ignition triggering.

6.2 Simulation of DDT

The coupled FTP methodology has been applied to the 2D numerical simulation of DDT in a PDE channel with flame accelerating obstacles and shock-wave focusing nozzle filled with the stoichiometric propane – air mixture at normal initial conditions.

Figure 14 shows the schematic of a planar PDE channel (channel height $H = 52$ mm, $L =$ 3 m) containing four segments: (1) flame acceleration segment 1280 mm long with one closed end and regular obstacles in the form of orifice plates with BR = 0.25 and pitch $S = 20$ mm, (2) first smooth-walled segment 220 mm long, (3) shock-wave focusing element 500 mm long in the form of the convergent-divergent (CD) nozzle of a special shape, and (4) second smooth-walled segment 1000 mm long with an end open to the atmosphere. The PDE configuration containing "flame accelerator" and "shock focusing element" has been first suggested in [21] for implementing a fast DDT concept [22, 23]. It implies that a shock wave generated by the accelerating flame can be transformed into a detonation wave while passing through a shock focusing element (tube coil, CD nozzle, etc.). The converging part of the CD nozzle ensures shock-to-detonation transition in the core flow downstream the nozzle throat, whereas the conical diverging part ensures detonation survival and transitioning to the smooth-walled channel of height H .

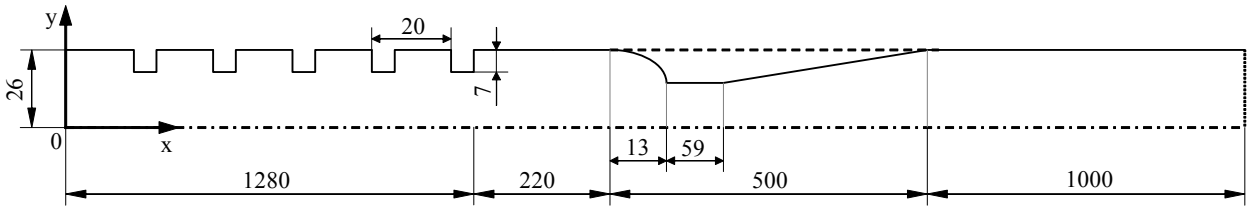

Figure 14: Schematic of a PDE tube with flame accelerator and shock focusing nozzle. Dimensions are in millimetres.

The first (intermediate) smooth-walled segment is used for ensuring a plug flow of shock-compressed unreacted mixture of duration sufficient for shock-to-detonation transition in the nozzle. The nozzle geometry was the same as that tested experimentally in [23] with the stoichiometric propane – air mixture.

The reactive mixture in the PDE channel was assumed initially quiescent and filling the entire geometry. The walls of the channel were assumed isothermal ($T_w = 293$ K). At the open end, a large-volume buffer section with initial pressure $p_0 = 1$ atm was attached to the PDE channel.

The boundary conditions and ignition were modeled in the same way as described above for the validation tests of the coupled FTP method. The ignition energy applied to the ignition kernel was 1 mJ. In planar 2D calculations, only an upper half of the PDE channel was considered with symmetry boundary conditions along three longitudinal symmetry planes. For tracing possible autoignition events, the preflame zone was filled with notional particles. The number of particles in each computational cell was controlled to be no less than 5 and no more than 20 with the mean value of 10. The autoignition of a particle was assumed to occur when the rate of temperature increase in this particle exceeded 10^6 K/s. The two-way coupling procedure between the particles and the mean flow was used. The autoignition of at least one particle in a cell was treated as the autoignition of all mixture throughout the cell volume.

Figure 15 shows the time histories of visible flame and lead shock wave velocities. In the flame acceleration segment, both the flame and lead shock velocities increase to about 980 m/s. Upon entering the first smooth-walled segment the flame starts decelerating whereas the shock wave continues accelerating and attains the velocity of 1400 m/s at the nozzle inlet. The diagram of Fig. 15 indicates shock-to-detonation transition in the nozzle. The detonation wave is initiated via the overdriven detonation

mode. The maximum degree of overdrive is 1.26. When the detonation wave enters the second smooth-walled segment, the degree of its overdrive is 1.03. The overdriven detonation further decays to the self-sustained CJ mode in the second smooth-walled segment with the constant velocity close to 1900 m/s. As mentioned above, this velocity corresponds to the thermodynamically equilibrium value calculated based on the truncated composition of reaction products in the 5-step mechanism of propane oxidation.

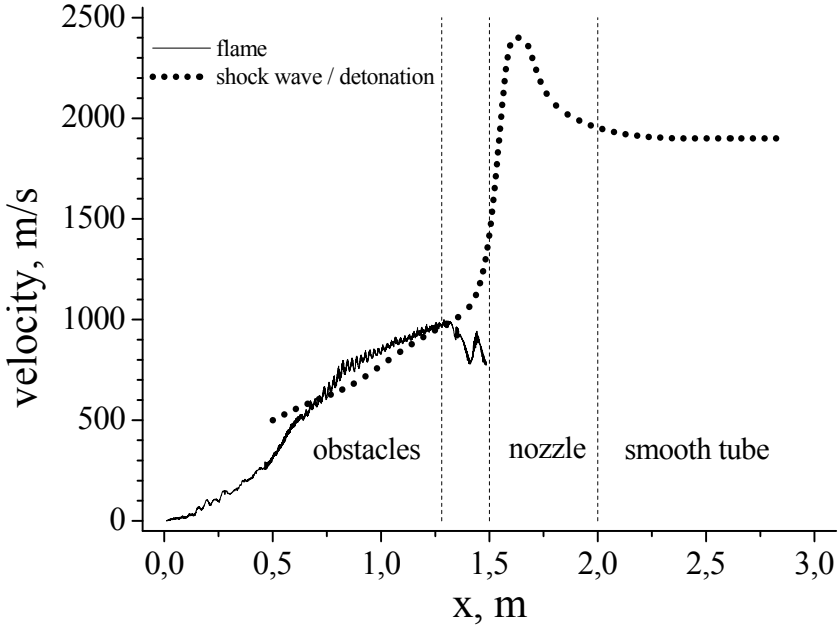

Figure 15: Flame (solid curve) and lead shock wave (dotted curve) velocities vs. distance.

Figure 16 shows the snapshots of temperature and pressure fields at several time instants ($t = 20$, 21, and 21.5 ms after ignition) during flame propagation in the flame accelerating segment. In the course of flame propagation along the channel its overall shape exhibits various transformations, including a tulip-like shape (not shown in Fig. 16) in qualitative accordance with experimental observations. Also seen are intense bow shocks attached to the obstacles which are the indication of supersonic shock-compressed flow ahead of the flame. Noteworthy is a short distance between the lead flame point and the flame-generated shock wave (about $1.2H$).

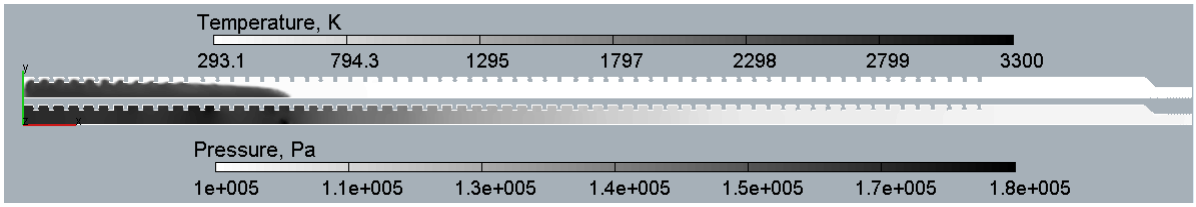

20 ms

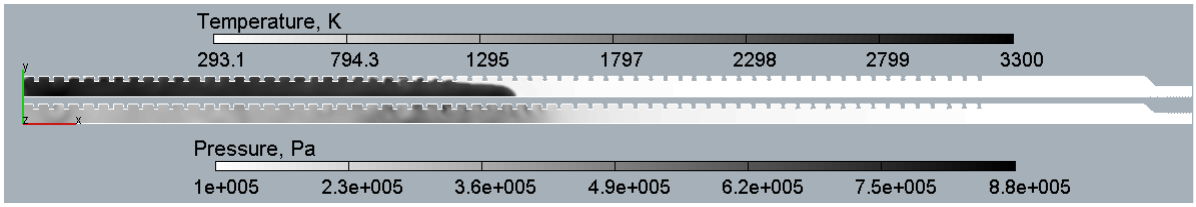

21 ms

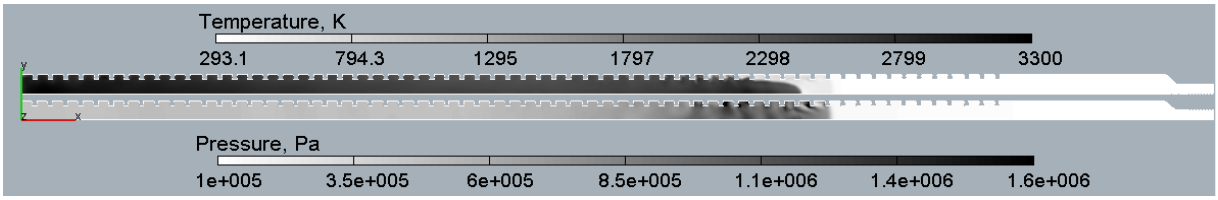

21.5 ms

Figure 16: Predicted temperature (top) and pressure (bottom) fields at $t = 20$, 21, and 21.5 ms.

Figure 17 is the continuation of the snapshot sequence in Fig. 16 for $t = 21.95$, 21.975, 22.0, and 22.025 ms after ignition. These snapshots correspond to the stage of the process after the shock wave – flame complex leaves the flame accelerating segment. At $t = 21.95$ ms, the shock wave – flame complex propagates in the first smooth-walled segment of the PDE channel. Due to lower turbulence intensity in this section, the flame lags behind the shock wave thus increasing the distance between them to about $2H$. At $t = 21.975$ ms, the shock wave reflects from the converging nozzle wall creating two clusters of exothermic centers clearly seen in both pressure and temperature snapshots. The hot spots are located at the converging nozzle surface. At $t = 22.0$ ms, the reflection-induced preflame autoignition ("explosion in the explosion" [24]) gives rise to an extended region with extremely fast volumetric combustion. This explosion generates an overdriven detonation in the rear and frontal parts of the region. The wave propagating towards the flame is usually referred to as a retonation wave: when passing through the flame it degenerates to a nonreactive shock wave propagating in the combustion products. The wave propagating outwards from the flame is referred to as a detonation wave. Contrary to the relatively slow initial stage of flame acceleration, the evolution of the DDT process after preflame autoignition is very fast and occurs within about 50 μs. Thus, in the presence of preflame autoignition, two modes of combustion become possible simultaneously, namely the frontal and volumetric.

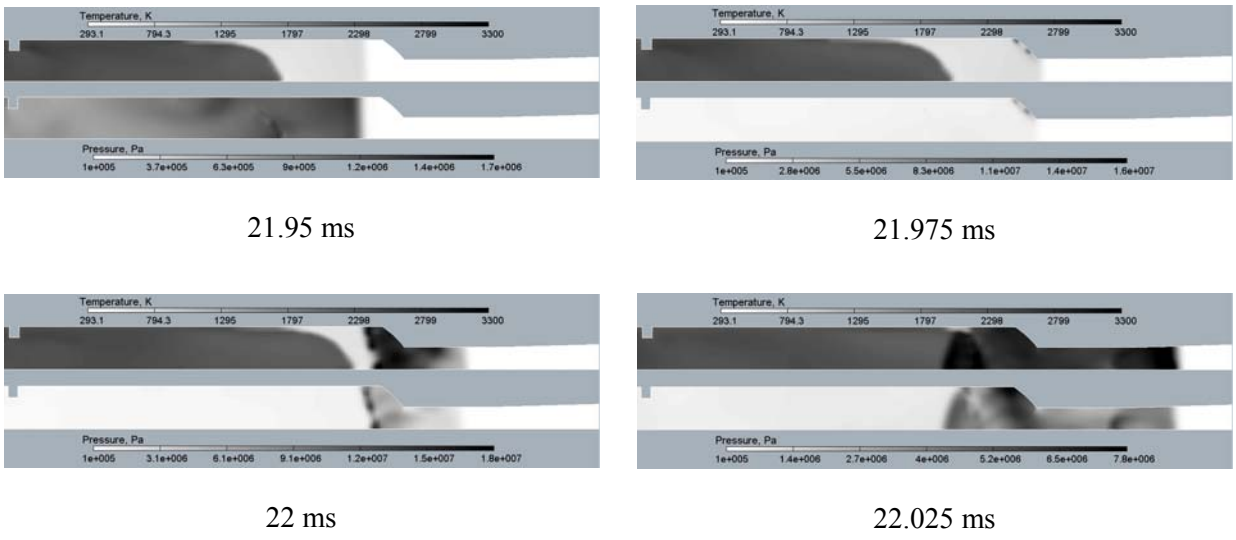

Figure 17: Snapshots of temperature and pressure fields prior, at and after shock-to-detonation transition (the transverse size of the tube is purposely increased to clarify the details).

Figure 18 shows the predicted spatial pressure distributions in the PDE channel at different time after ignition. Pressure oscillations are caused by bow shocks and rarefaction waves generated by regular obstacles. The localized "explosion in the explosion" occurring at about 22 ms results in pressure rise up to 150 atm. Figure 19 shows the snapshots of temperature and pressure corresponding to all time instants presented in Fig. 18.

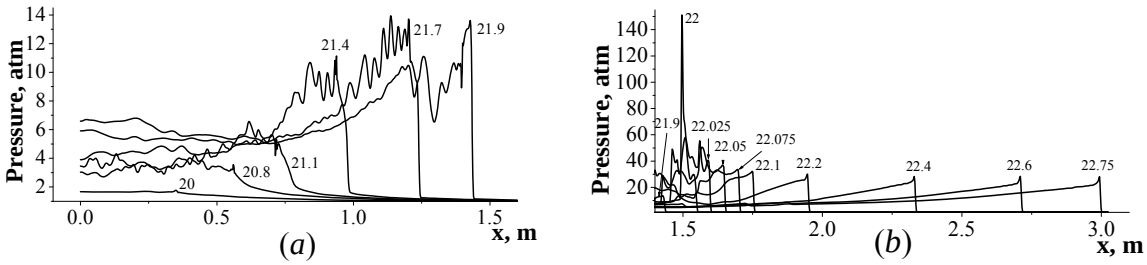

Figure 18: Predicted spatial pressure distributions in the PDE channel at different time (in ms) after ignition. Different pressure scales are used for $t < 21.9$ (*a*) and $t > 21.9$ ms (*b*).

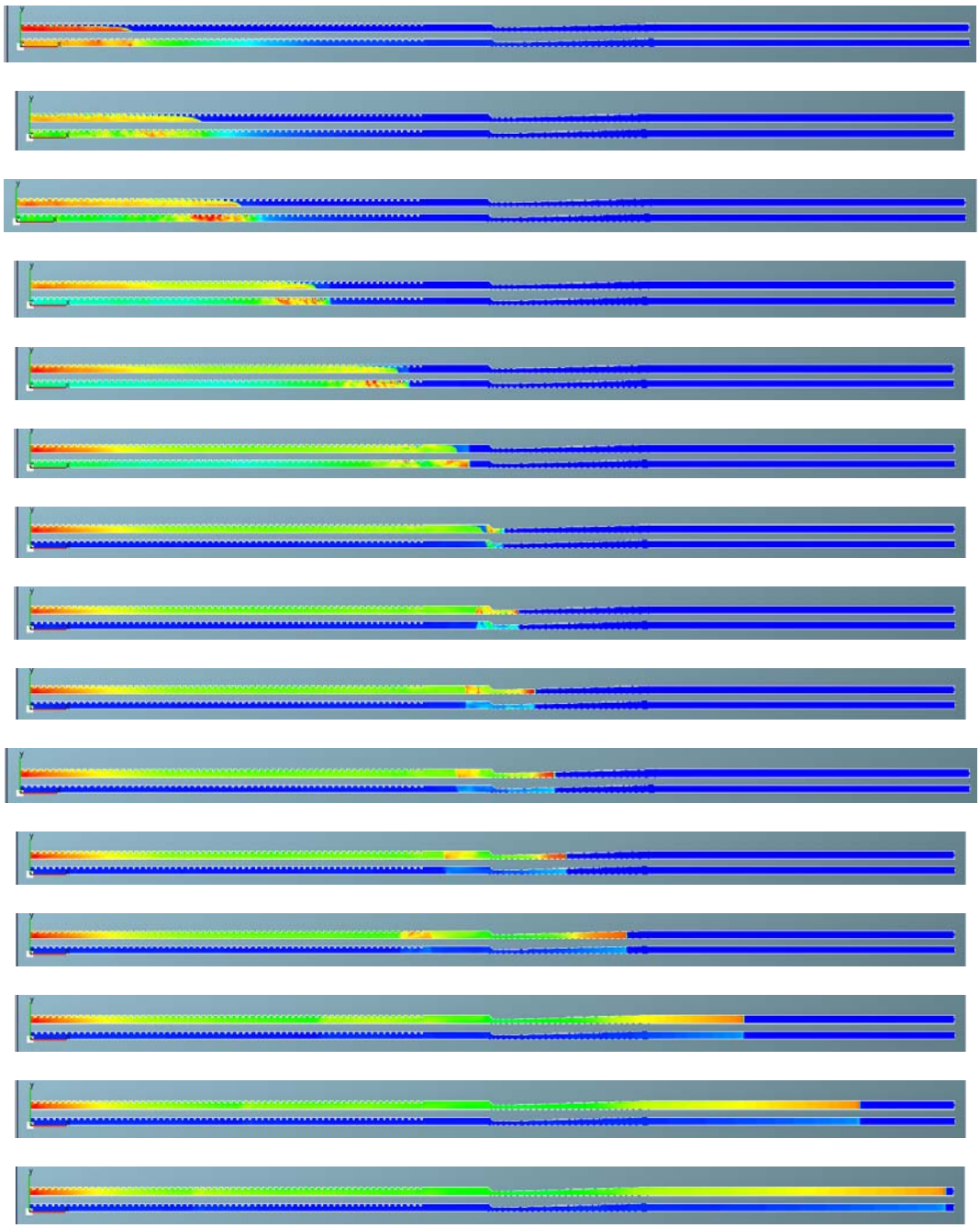

Figure 19: Predicted temperature (top) and pressure (bottom) fields at different time (in ms) after ignition (snapshots correspond to time instants shown in Fig. 18).

6.3 Thrust Performance

Let us analyze the thrust performance of the nonidealized PDE under study.

The dashed curve in Fig. 20 shows the time history of the specific (per unit area) thrust defined by Eq. (7). As before, for the sake of convenience, Fig. 20a shows the specific thrust history for the early stage of the exhaust process ($t < 12$ ms) and Fig. 20b for its late stage ($9 < t < 50$ ms). The impulse I (see Eq. (8)), i.e., the area under the dashed curve in Fig. 20, is approximately 4880 $\mathrm{Pa \cdot s}$. The estimated calculation

error of I is 2%, i.e., $I \approx 4880 \pm 100$ Pa·s. Taking into account that for the PDE channel of Fig. 14 F_e = 0.026 m^2/m, $m_f \approx 0.0052$ kg/m, and $g = 9.8$ m/s^2, one comes to the following value of the specific impulse I_{sp}:

$$I_{sp} = F_e \frac{R}{m_f g} \approx 0.026 \frac{4880}{0.0052 \cdot 9.8} \approx 2480 \pm 50 \text{ s} \tag{16}$$

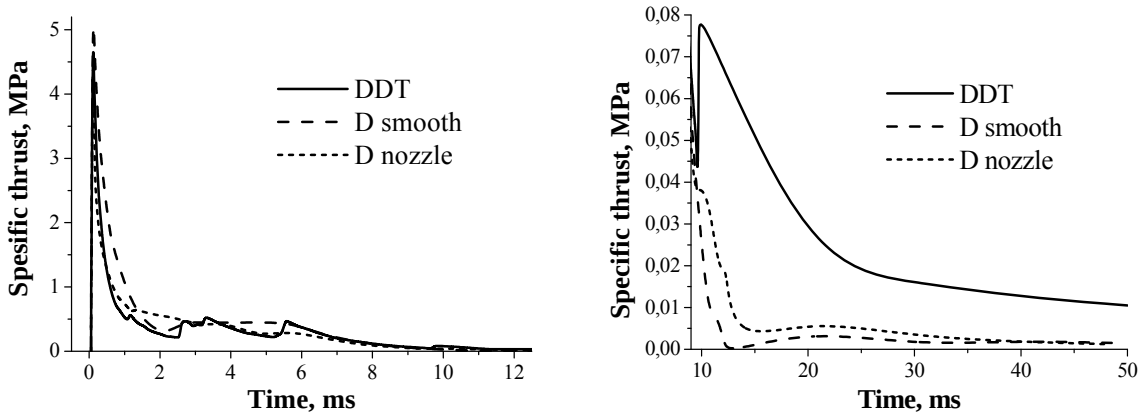

(a) (b)

Figure 20: Time histories of the specific (per unit area) thrust calculated based on the exhaust flow parameters at the PDE channel exit: solid curve – direct detonation initiation in a straight smooth-walled channel; dashed curve – DDT in the PDE channel of Fig. 14, dotted curve – direct detonation initiation in the PDE channel of Fig. 5: (a) $t < 12$ ms, (b) $9 < t < 50$ ms.

Note that this value has been obtained based on Eqs. (7)–(9), i.e., based on momentum integration at the PDE outlet. Thus, the value of 2480 ± 50 s should be treated as the net specific impulse at PDE full fill conditions.

This value of the specific impulse should be identical to the value obtained by direct integration of the pressure over the projection of all PDE channel surfaces on the plane normal to y-axis. However, if one integrates the pressure only over the PDE thrust wall (left end of the PDE channel in Fig. 14), the arising difference between the two values of the specific impulse can be attributed to momentum and energy losses.

Figure 21 shows the calculated time history of pressure p_T at the thrust wall. Using Eqs. (10) and (11) for defining the force acting at the unit area of the thrust wall P_T and impulse per unit area I_T, one obtains

$$I_{sp,T} = F_T \frac{I_T}{m_f g} \approx 0.026 \frac{5060}{0.0052 \cdot 9.8} \approx 2580 \text{ s}$$

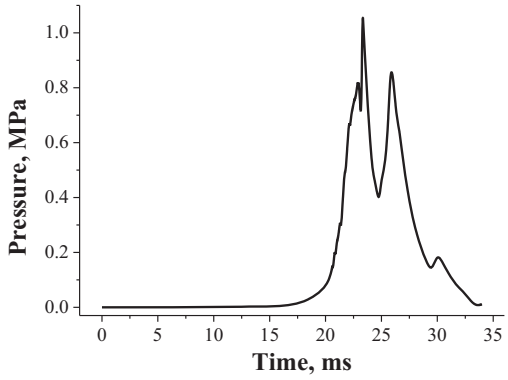

Figure 21: Predicted absolute pressure history at the head end of the PDE tube (PDE thrust wall).

Since the value of $I_{sp,T}$ is calculated more precisely than I_{sp}, the difference between these values can be estimated as $\Delta I_{sp} = I_{sp} - I_{sp,T} \approx -100 \pm 50$ s. This difference should be obviously attributed to momentum and energy losses in the PDE channel flow caused by obstacles, CD nozzle, and cold walls. The relative contribution of the losses is unexpectedly very small: $\Delta I_{sp} / I_{sp} \approx 2\% - 6\%$. By other words, the specific impulse of the PDE under study can be estimated based on the thrust wall pressure p_T.

It is interesting that the value of I_{sp} given by Eq. (16) is nearly the same as that given by Eq. (13), i.e., the DDT process in the PDE channel with obstacles and CD nozzle provides the same specific impulse as a detonation in a straight channel of the same length and nearly the same fuel mass. One has to take into account that contrary to the I_{sp} of Eq. (16) the value of I_{sp} of Eq. (13) is affected by the contribution of detonation initiator [13].

For the PDE configuration of Fig. 14, an additional calculation was made: instead of DDT, direct detonation initiation was applied. The initiation technique was the same as in Fig. 5. The specific thrust history at the PDE channel outlet for this case is shown by the dotted curve in Fig. 20. Since the area under the dotted curve in Fig. 20 is approximately equal to $I \approx 4180 \pm 80$ Pa·s and $m_f \approx 0.0052$ kg/m, the calculated value of I_{sp} is equal to

$$I_{sp} = F_e \frac{I}{m_f g} \approx 0.026 \frac{4180}{0.0052 \cdot 9.8} = 2130 \pm 40 \text{ s}$$

which is considerably (by 12%) less than the value of $I_{sp} \approx 2480 \pm 50$ s obtained for DDT. This unambiguously means that overall momentum and energy losses at direct detonation initiation are higher than at DDT, in particular in the obstructed segment of the PDE channel. Since the momentum losses are proportional to ρU^2, propagation of detonation in this segment of the channel is accompanied with higher momentum losses than in the course of flame acceleration. As for the intensity of heat losses, it is known to be higher for flows with higher Reynolds number, i.e., in a detonation wave. It is noteworthy that detonation requires a much shorter time for channel evacuation than a DDT.

7.0 PDE PERFORMANCE IN FLIGHT CONDITIONS

To study the PDE thrust performance in flight conditions, we considered a PDE-based axisymmetric vehicle of Fig. 4 with supersonic air intake, bypass channel, mechanical valve, and nozzle, flying at M_∞ = 3.0 at the altitude 9.3 km. At this altitude, the approach air-stream static temperature is 228 K giving the speed of sound of 303.6 m/s, and the static pressure is 0.29 atm.

The specific geometrical dimensions of the vehicle under consideration are given in Fig. 22. The total length of the vehicle is 1829 mm, the outer diameter is 83 mm. The detonation chamber is a cylindrical tube 52 mm in inner diameter with regular obstacles in the form of orifice plates (BR = 0.3). A supersonic nozzle with the throat 36 mm in diameter is attached to the right end of the detonation chamber. Due to the specific shape of the bypass channel entrance, the mechanical valve blocks 73% of the engine-duct cross section when the entrance to the detonation chamber is closed and 48% when it is open.

The engine was assumed to be fueled with gaseous propane. In the calculations, propane was supplied to the flow through the computational cells ("feed" cells) in a chosen cross section of the detonation chamber (shown as a vertical line marked in red in Fig. 22) by making a provision for a proper mass source in the cells. The chosen value of the mass source ensured the stoichiometric mixture composition in the "feed" cells. Ignition was triggered in the wake of the first orifice plate as shown in Fig. 22. The ignition procedure was the same as described above for the validation tests of the coupled FTP method. The ignition energy was on the order of 1 mJ.

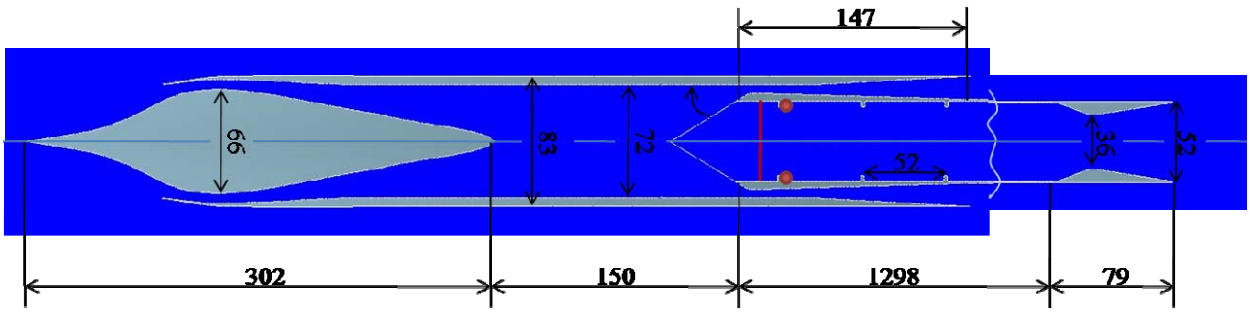

Figure 22: Flying PDE-based vehicle. Dimensions are in millimeters.

Figure 23 shows the predicted time history of PDE thrust in the course of three engine cycles. As follows from Fig. 23, the first cycle differs considerably from the subsequent cycles, whereas the second and third cycles are nearly identical. Thus, the operation process becomes reproducible (attains the limiting cycle conditions) after the second-third cycle and engine thrust performance can be evaluated starting from the second or third cycle. The first cycle is different from the subsequent cycles due to the difference in the initial conditions for the first and subsequent cycles. Actually, the duration of the first cycle is 14 rather than 10 ms characteristic for the second and third cycles.

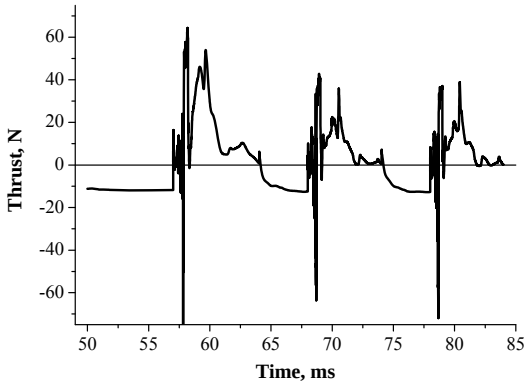

Figure 23: Predicted time history of PDE thrust in the course of three engine cycles.

The drag force can be evaluated by considering the flow in the PDE duct without combustion. Thus, in the third cycle the components of the drag force impulse are:

–0.04090 $\mathrm{N \cdot s}$ (filling stage; valve is open; duration 4 ms)

–0.02855 $\mathrm{N \cdot s}$ (purging of bypass channel with air; valve is closed; duration 6 ms)

The drag force at the filling stage is –0.04090/0.004 = –10.225 N, whereas the drag force at the stage of air purging through the bypass channel is –0.02855/0.006 = –4.758 N. Taking into account that these drag force components act during 0.4 and 0.6 fractions of the total cycle time, respectively, one obtains for the average drag force in the third cycle: $-(10.225 \cdot 0.4 + 4.758 \cdot 0.6) = -6.945$ N.

Now, the PDE thrust can be estimated as the sum of the net force and the average drag force: 0.436 + 6.945 = 7.381 N.

To estimate the specific impulse, one has to take into account that the mass of fuel supplied to the detonation chamber in the third cycle is $4.92 \cdot 10^{-6}$ kg. Thus, the specific impulse is equal to

$$I_{sp} = \frac{7.381 \cdot 0.01}{4.92 \cdot 10^{-6} \cdot 9.8} \approx 1531 \pm 100 \text{ s}$$

Similar estimates for the second cycle give the value of $I_{sp} \approx 1600$ s. In view of the difference between the I_{sp} values at the second and third operation cycles and accompanying estimation errors, we come to the conclusion that $I_{sp} \approx 1550 \pm 100$ s. This value is lower than that obtained above for zero flight speed (2480 ± 50 s) but still higher than for a typical ramjet.

It is instructive to look at the flow pattern in the PDE at flight conditions. Figure 24 shows the predicted response of the flow in the engine receiver to a change in the valve position in terms of static pressure isolines. This figure is plotted for the second cycle of PDE operation. When the valve is open (Fig. 24a) the bypass channel is closed and the entire airflow goes through the detonation chamber where it is mixed with fuel.

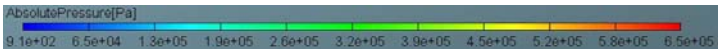

(a) 68 ms

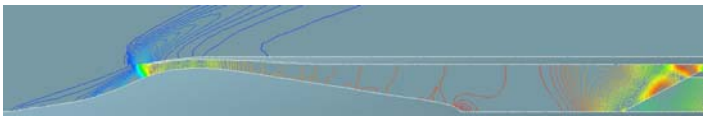

(b) 68.1 ms

(c) 68.4 ms

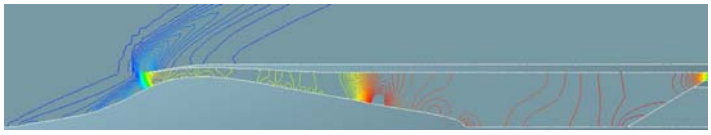

(d) 68.7 ms

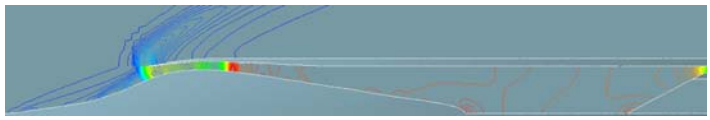

(e) 69 ms

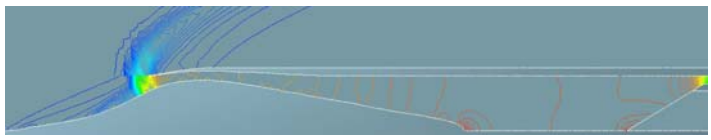

(f) 69.5 ms

(g) 70 ms

(h) 74 ms

Figure 24: Predicted response of the flow in the engine receiver to a change in the valve position in terms of static pressure isolines.

Figure 24b shows the flow field 0.1 ms after the valve is instantaneously closed. Valve closing results in the formation of pressure waves propagating downstream in the bypass channel and upstream in the receiver (Figs. 24b and 24c). The latter penetrates into the intake (Figs. 24d and 24e) and approaches the normal shock at the intake entrance (Fig. 24f, 24g, and 24h) without disturbing much the flow therein.

The duration of the flow through the bypass channel is 6 ms. This time corresponds to the active stage in the detonation chamber. During this transient period, the flow in the intake does not change its direction. Subsequent instantaneous valve opening results in flow transformation to the pattern shown in Fig. 24a.

The duration of the flow through the detonation chamber is 4 ms. This time corresponds to purging and filling stages of the operation process. Thus, the total cycle time in this example is 10 ms and the operation frequency is 100 Hz. The characteristic airflow parameters at the axis of the receiver in Fig. 24g are: pressure – approximately 6.9 atm, temperature – approximately 600 K, and flow velocity – approximately 100 m/s.

Consider now the processes in the detonation chamber. Figure 25 demonstrates the flow patterns in the course of chamber filling with fuel (Fig. 25a), flame propagation shortly after ignition (Fig. 25b) and at a later stage, when flame accelerates considerably (Fig. 25c), shortly prior to DDT (Fig. 25d) and shortly after DDT (Fig. 25e), as well as during detonation wave propagation in the chamber (Fig. 25f).

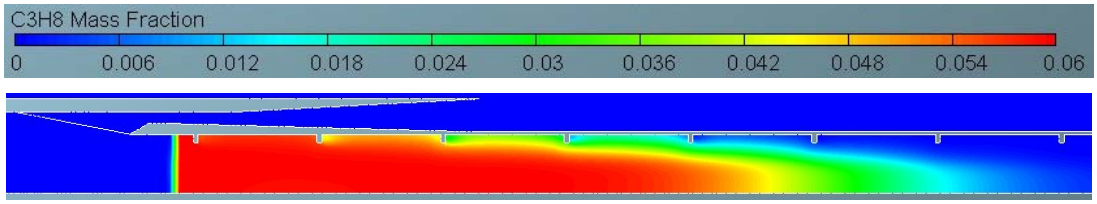

(a) 65 ms

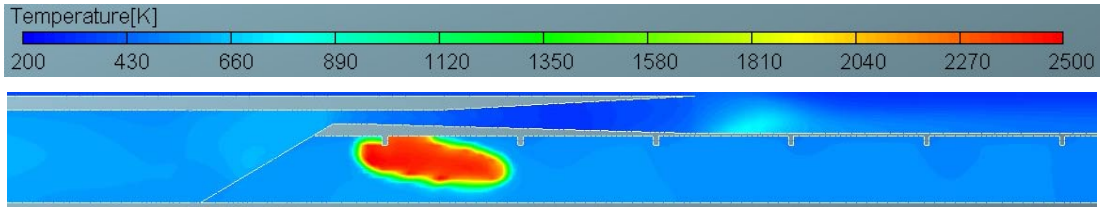

(b) 68.2 ms

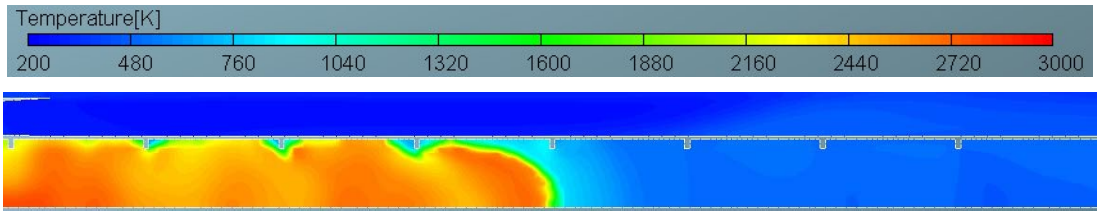

(c) 68.58 ms

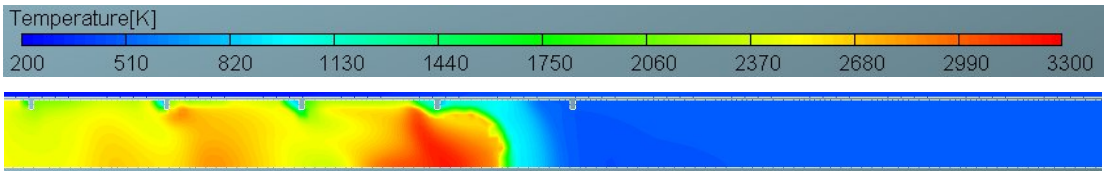

(d) 68.68 ms

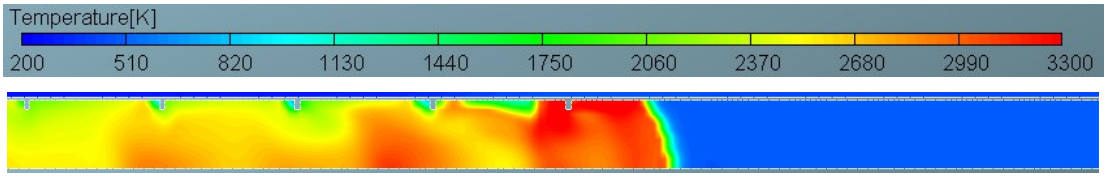

(e) 68.7 ms

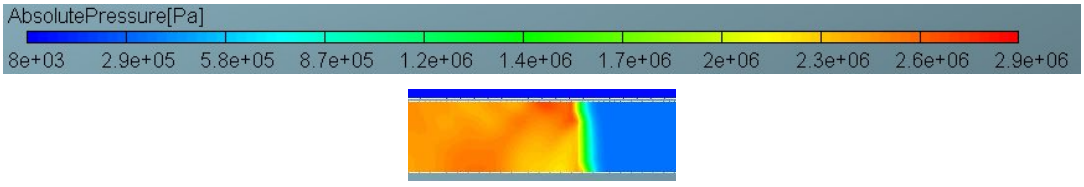

(f) 68.88 ms

Figure 25: Flow patterns at detonation chamber filling with fuel (a), flame propagation shortly after ignition (b) and at a later stage, when flame accelerates considerably (c), as well as shortly prior to DDT (d) and shortly after DDT (e), and at detonation propagation in the detonation chamber (f).

Careful consideration of Fig. 25f reveals the existence of several transverse waves in the detonation front structure indicating that the detonation propagates in conditions far from the detonability limit. As a matter of fact, the flow parameters in front of the detonation wave in Fig. 25f are: mixture composition – stoichiometric, pressure – 5 atm, temperature – 530 K, flow velocity at the chamber axis – 250 m/s, and mean pulsating velocity – 30–40 m/s. Despite the chamber diameter (52 mm) is close to the limiting tube diameter for the detonation of stoichiometric propane – air mixture at normal initial conditions, the elevated pressure and temperature in the chamber highly promote detonation sensitivity of the explosive composition.

Figure 26 shows flow patterns in the nozzle of the PDE-based vehicle and in the exhaust plume at several time instants during the second operation cycle. One can clearly observe cooling of detonation products during expansion in the supersonic nozzle. Despite the reflection of the detonation wave from the converging nozzle section temporarily produces a negative thrust component the supersonic nozzle is needed to provide a necessary level of backpressure in the detonation chamber. After the detonation wave emanates from the nozzle, a transient wave system is formed downstream. This system includes a strong bow shock attached to the nozzle edge and a traveling Mach disk arising at a distance of about 4 nozzle exit diameters (Fig. 26a) and decaying at about 7 nozzle exit diameters (Fig. 26b and Fig. 26c). The maximum transverse size of the plume is about 4 nozzle exit diameters.

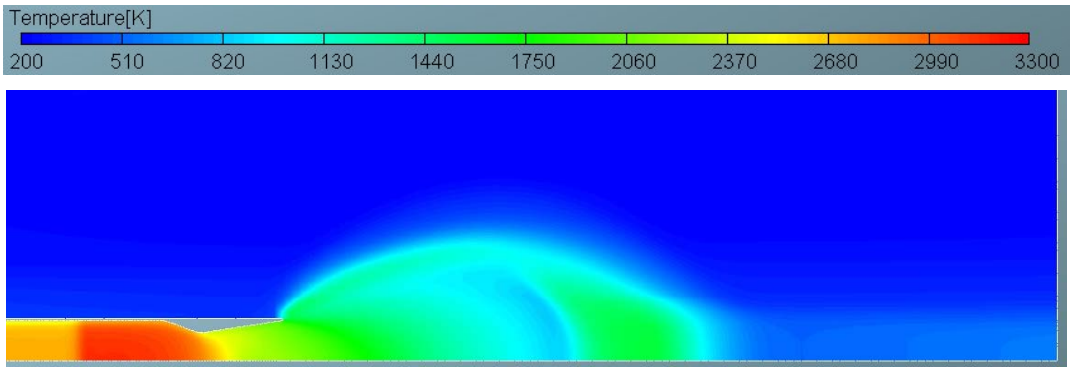

(a) 69.2 ms

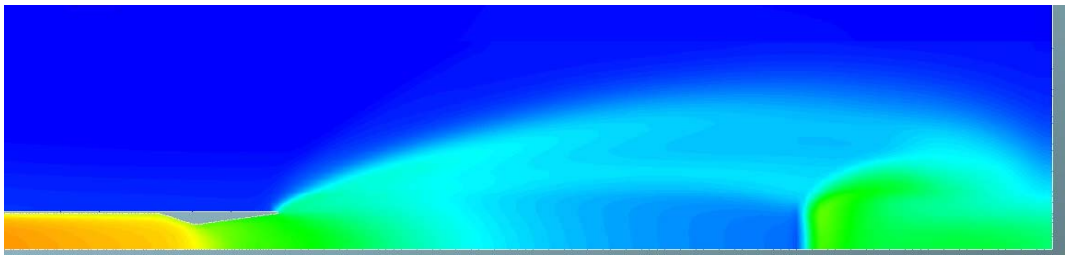

(b) 69.4 ms

(c) 70 ms

Figure 26: Flow patterns in the nozzle of the PDE-based vehicle and in the exhaust plume.

8.0 EXPERIMENTAL SUBSTANTIATION

8.1 Preliminary Remarks

Thus, it has been shown above that the fuel-based specific impulse for the propane-fueled air-breathing PDE at Mach 3.0 flight conditions is $I_{sp} \approx 1550 \pm 100$ s, which is higher than the specific impulse characteristic for hydrocarbon-fueled ramjets. The DDT run-up distance and time in such conditions were predicted to be so short that the engine integrating the supersonic intake, detonation chamber, bypass channel, valve distribution system, and supersonic nozzle could be quite compact with the total length as short as about 1.8 m and could operate at the altitude of 9.3 km with positive thrust at a frequency of 100 Hz and very low detonation ignition energy on the order of 1 mJ.

The possibility of obtaining a repeatable DDT in hydrocarbon fuel – air mixture with such short run-up distances and times at the ignition energy at such a low level has been experimentally studied at the SICP. Several engine designs have been suggested and PDE demonstrators fabricated and tested. Some examples and results are discussed below in this Section.

8.2 Research PDE Demonstrator

In 2005, a liquid-fueled air-breathing Research PDE (RPDE) demonstrator has been developed at SICP in Moscow. The demonstrator operation principles and performance were discussed in detail in [21]. A schematic diagram of the RPDE is shown in Fig. 27.

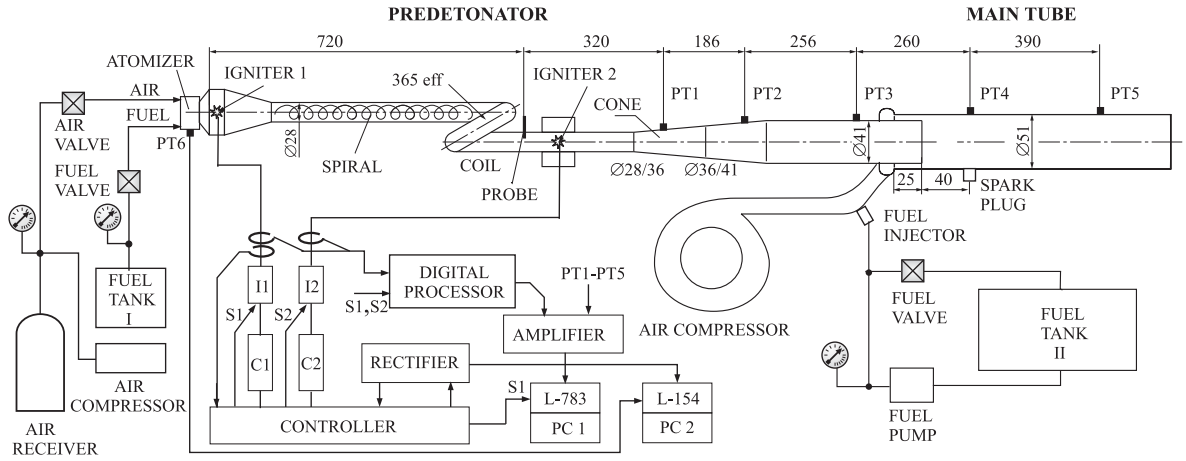

Figure 27: The Semenov Institute RPDE demonstrator.

The RPDE consisted of a predetonator and a main tube. The predetonator was a combination of two tubes, 28 and 41 mm in diameter connected by a tapered transition section. The fuel atomizer at one end of the 28-millimeter-diameter tube produced very fine droplets (5–6 μm at a distance of 70 mm from the nozzle). A low-energy electrical ignition system was used to ignite the resulting two-phase flow at a position 60 mm downstream from the atomizer. A 400-mm-long Shchelkin spiral inserted in the tube was used for accelerating the arising flame to the visible velocity on the level of 600 to 700 m/s. The straight portion of the predetonator was connected to a single coil of 365-mm length. The shock wave produced by the accelerating flame propagated through the coil and subsequently emerged as a detonation wave in a second straight section of 28-millimeter-diameter tube. Interaction of the shock wave with the coil walls generated a transverse wave which transitioned into a single-head spinning detonation. The detonation propagated through the tapered section into the 41-mm-diameter portion of the predetonator tube. It

subsequently transmitted to the 51-millimeter-diameter main tube which was supplied with a fuel–air mixture through the annular gap between the predetonator and main tube.

The fuel–air mixture in the main tube was supplied by a low-head compressor in conjunction with a standard automotive fuel injector that produced droplets in the 70–80-μm range. The fuels tested included *n*-hexane and *n*-heptane. Under cold start-up conditions, only a shock wave emerged from the coil (rather than a detonation wave), and a second igniter (igniter 2 in Fig. 27) was fired at the precise moment the shock wave traversed it, resulting in initiation of detonation. The second igniter was not required after seven to eight detonation pulses. Stable operation was observed after 12–15 pulses.

The minimal mean fuel–air ratio in the predetonator required for the cold start-up of the RPDE was 1.3 ± 0.1. The need in the fuel-rich mixture was attributed to the partial deposition of the injected fuel on the cold inner wall of the tube. After the transient initial period of operation, the optimal fuel–air ratio in both the predetonator and the main tube approached the stoichiometric value. This observation was based on the measurements of fuel consumption rate in experiments with the initially hot tube. Air and fuel flow rates in the detonation mode measured in the predetonator were 6.7 ± 0.5 and 0.4 ± 0.1 g/s, respectively; and in the main tube, 60 ± 7 and 3.8 ± 0.1 g/s, respectively. Due to the existence of two fueling zones there could be some overlap between them downstream from the entrance to the main tube. However, as the mass flow rates of fuel in the predetonator were about the order of magnitude less than in the main tube, this issue was not particularly addressed.

The design of the RPDE was optimized in terms of obtaining the lowest possible ignition energy and shortest length. The rated ignition energy required for DDT was as low as 24 J. This energy was calculated based on the capacitance and voltage at igniter capacitors. Taking into account the residual energy in the capacitors after electrical discharge, the maximal error in determining the ignition energy did not exceed 7%. The efficiency at which electrical energy was deposited into the working fluid was about 15%–20%. At rated ignition energies below 24 J, ignition of the two-phase mixture failed due to flame blow-off from the igniter electrodes and reaction quenching. The total length of the system was 2.2 m. The plume of the predetonator is shown in Fig. 28. One can clearly see the multiwave structure of the supersonic exhaust plume.

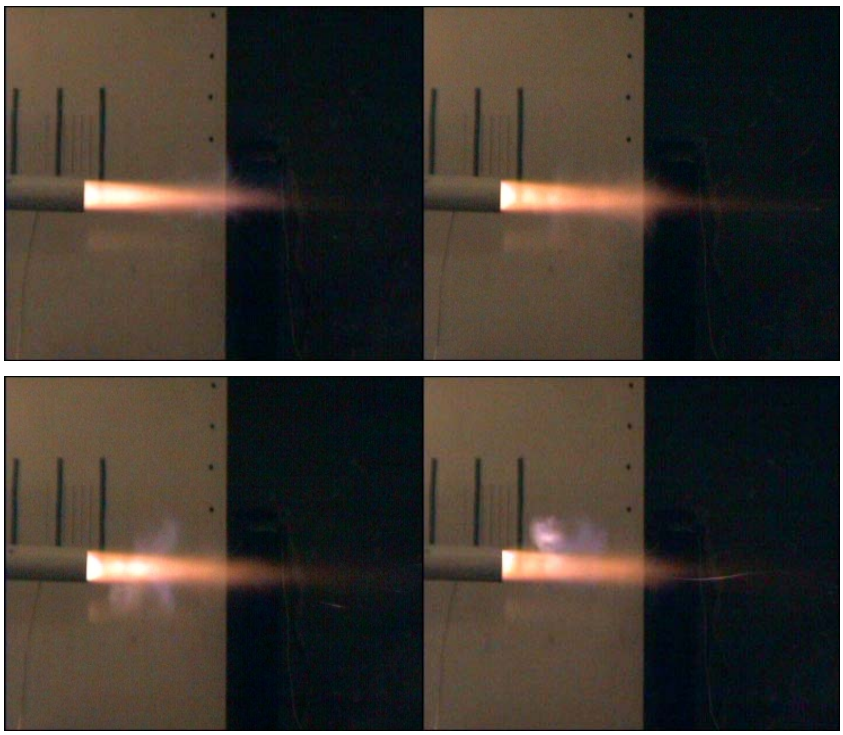

Figure 28: The plume of the RPDE in four successive pulses.

The RPDE design was optimized for attaining stable operation in the detonation mode rather than for obtaining high thrust performance. It was fired at a very low operation frequency (2.2–3.9 Hz). Nevertheless, a specific impulse of 700–800 s was gained at static conditions, which is roughly a half of the specific impulse relevant to hydrocarbon-fueled ramjets at Mach 2 flight conditions. The obtained value of the specific impulse is mainly explained by incomplete fuel combustion caused by low operation frequency and short main tube. However, owing to acceptable weight and size characteristics of the demonstrator, the proposed process design was regarded as promising for practical applications.

In 2005, when the demonstrator was tested, the main problems to be solved were to ensure the stable operation of the RPDE that burned low-volatile fuel of the type of aviation kerosene rather than high-volatile fuel (*n*-hexane and *n*-heptane) and to increase the delivered specific impulse by optimizing the length of the main tube and the operation frequency.

The main advantage of the RPDE design under consideration was that it was based on DDT rather than direct detonation initiation. Moreover, in this design, no supplemental oxygen was required for successful predetonator operation.

8.3 Kerosene-Fueled Predetonator with Curved Tube Segment

The main element of the RPDE of Section 7.1 is the predetonator which ensures DDT at the shortest possible length with the lowest possible ignition energy. In 2006, a kerosene-fueled air-breathing predetonator has been developed at the SICP. The predetonator operation principles and performance were discussed in detail in [22]. A schematic diagram of the system is shown in Fig. 29.

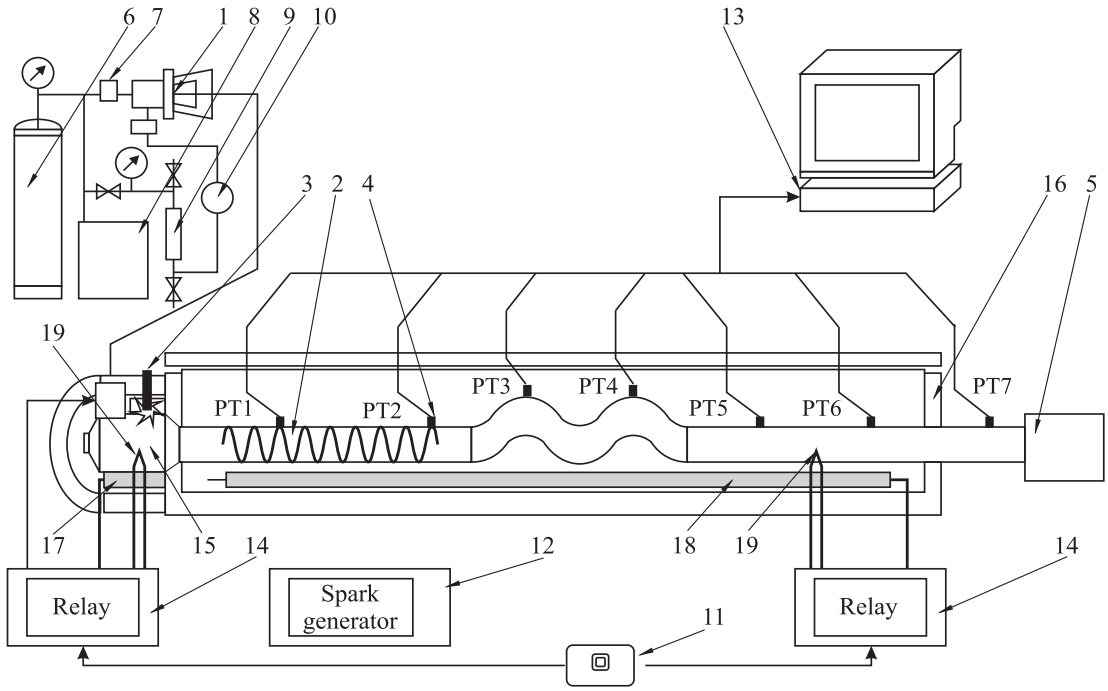

Figure 29: Kerosene-fueled predetonator with curved tube segment.

The predetonator comprised kerosene injector *1*, detonation tube *2*, electrical igniter *3*, pressure transducers *4*, detonation arrester *5*, air bottle *6*, fuel valve *7*, air compressor *8*, kerosene tank *9*, fuel filter *10*, digital controller *11*, power supply *12*, PC *13*, control relay *14*, prevaporizer *15*, thermostat *16*, electrical heaters *17* and *18*, and thermocouples *19*. The fuel and air supply system provided the supply of fuel mixture components (liquid kerosene TS-1 — Russian analog of JetA — and air) in constant proportion due to the same driving pressure. Mixing of fuel and air started in the air-assist atomizer *1* and terminated in the detonation tube *2* of internal diameter 52 mm and 3 m long.

The detonation tube was equipped with the igniter *3*, water-cooled high-frequency pressure transducers PT1 to PT7 and/or ionization probes. The air-assist atomizer provided very fine kerosene drops 5 to 10 μm in diameter. Drop size distribution was measured by a soot-sampling method. The air was fed from the air bottle *6* connected to air compressor *8*. The two-phase fuel-air mixture was continuously injected to the prevaporizer section *15* of the detonation tube *2*. In this section, kerosene drops were partly vaporized and the hybrid drop – vapor – air mixture followed to the tube section with the Shchelkin spiral and shock-focusing elements with low hydraulic resistance. The mass flow rate of the fuel–air mixture through the prevaporizer was varied from 12 to 20 l/s. To the end of the detonation tube, a detonation arrester was attached, which was a piece of 80-mm tube filled with the roll of thin corrugated metal tape.

The external heating system was used to avoid the starting procedure. The heating system consisted of the thermostat with the prevaporizer *15* and the thermostat *16* with the detonation tube.

The thermostats were equipped with electrical heaters *17* (0.6 kW) and *18* (2.5 kW), as well as with thermocouples *19*. The thermostats were controlled by the control relays *14*. The data acquisition system was based on analog-to-digital converter and a PC *13*. The total number of registration channels was 16. The predetonator was operated remotely.

Two sets of tests with the predetonator have been made. In the first, the detonation tube was straight, while in the second it contained a curved segment as shown in Fig. 30. The length of the Shchelkin spiral in both detonation tubes was 800 mm. The spiral was mounted 70 mm downstream from the prevaporizer nozzle.

In the tests with both tubes, the prevaporizer wall temperature was 190±10 °C. The temperature of the tube segment with the Shchelkin spiral was 120–130 °C and the temperature of the tube segment up to pressure transducer PT6 was 110–120 °C. The temperature of the tube segment downstream from pressure transducer PT6 was 20–30 °C.

The fuel–air mixture was ignited in the prevaporizer either by the standard spark plug or by a more powerful electric discharge. In the tests with the straight tube, the ignition energy was varied from 5 to 700 J. In these tests, the maximum registered shock wave velocity was about 800 m/s, i.e., no DDT was obtained.

The second test series was performed with the curved tube of Fig. 30. The idea of using such a curved tube comes from the work on RPDE of section 6.1, where the combination of Shchelkin spiral followed by the tube coil was shown to be very efficient for shortening DDT distance and time. The curved tube segment consisted of two complete turns of the tube with the external diameter of 57 mm tightly around a rod 28 mm in diameter with the pitch of 255 mm.

Figure 30 The curved tube segment in the thermostat.

The curved tube segment was mounted 100 mm downstream from the end of Shchelkin spiral. In the experiments with the curved tube segment the ignition energy was varied from 0.1 to 176 J. In these experiments, we have repeatedly registered detonation even at the lowest ignition energy used (0.1 J). Figure 31 shows the example of pressure records by pressure transducers PT1 to PT7 at the ignition energy of 0.1 J indicating the onset of detonation.

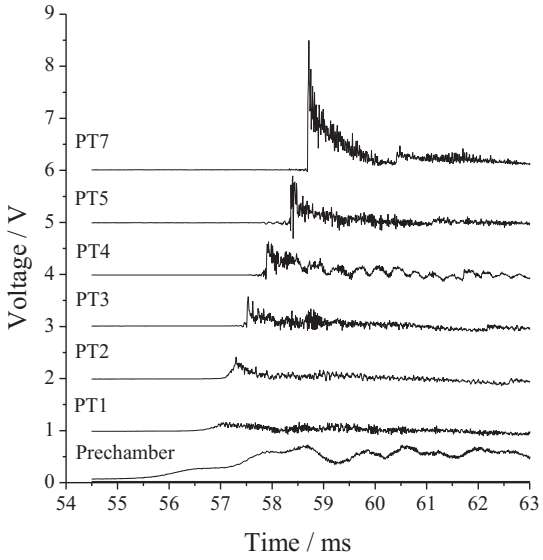

Figure 31: Example of pressure records by transducers PT1 to PT7 at ignition energy 0.1 J indicating the onset of detonation.

Table 1 shows the measured mean shock wave velocities along the detonation tube in 20 successive shots during multipulse operation of the predetonator. In all pulses, DDT in kerosene – air mixture was repeatedly attained at a distance of about 2 m with the propagation velocity at measuring segments (MS) PT5–PT6 and PT6–PT7 in the straight tube section on the level of 1830 ± 100 m/s despite a relatively poor pulse-to-pulse reproducibility of the shock-wave velocity at MSs PT1–PT2, PT2–PT3, and PT3–PT4 prior to DDT at MS PT4–PT5. The DDT was solely attributed to the use of the curved tube segment. The curvilinear reflecting surfaces in the curved tube led to gas-dynamic focusing of compression waves generated by the accelerating flame [22].

Table 1: Measured shock wave velocities (in m/s) at different measuring segments of the predetonator in 20 successive pulses at operation frequency 1.5 Hz.

Pulse No.	PT1–PT2	PT2–PT3	PT3–PT4	PT4–PT5	PT5–PT6	PT6–PT7
1	912	952	1014	1182	1852	1734
2	912	987	1105	1633	1961	1852
3	784	1020	1139	1690	1852	1841
4	947	955	1073	1690	1841	1744
5	929	952	1105	1633	2113	1639
6	791	1064	1457	1752	1734	1852
7	822	1095	1138	1633	1841	1744
8	746	1017	1402	1678	1875	1734
9	850	1017	1402	1633	1974	1734
10	725	1141	1581	1690	1841	1744
11	725	1095	1588	1690	1841	1852
12	702	1141	1729	1633	1852	1840
13	631	1136	1588	1752	1734	1744
14	648	1186	1652	1752	1734	1744
15	746	1056	1588	1690	1734	1961
16	702	1020	1588	1627	1852	1840
17	587	987	1652	1633	1974	1734
18	723	926	1457	1690	1840	1852
19	912	896	1652	1690	1744	1840
20	725	822	1138	1627	1852	1852

The predetonator was optimized for attaining stable multipulse operation in the detonation mode rather than for obtaining high thrust performance. Despite the DDT run-up time in this predetonator was quite short (6–7 ms), implying a possibility of high-frequency operation (up to 50-60 Hz taking into account its filling and purging), it was fired only at low operation frequencies of 1–3 Hz.

8.4 Kerosene-Fuelled Predetonator with CD Nozzle

In 2009, another kerosene-fuelled predetonator has been developed at the SICP in Moscow. In this predetonator, instead of the shock-focusing element in the form of the curved tube segment, a CD nozzle insert was used. A schematic diagram of the system is shown in Fig. 32.

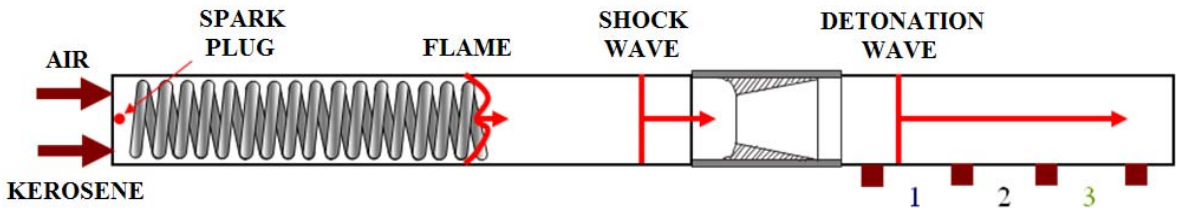

Figure 32: Kerosene-fueled predetonator with a CD nozzle as a shock-focusing element.

This system is similar to that considered in Fig. 14. Firing of this predetonator in the multipulse mode showed that it reliably provides DDT at short run-up distances (shorter than 2 m) and times (5–6 ms) with energy requirements as low as 0.1 J. Figure 33 shows the measured shock wave velocities at three MSs (1

to 3 in Fig. 32) in 10 successive pulses. One can see that the measured shock wave velocity at MS-2 and MS-3 in all pulses is nearly constant and attains the value of 1700–1800 m/s close to the CJ detonation velocity in kerosene – air mixture. The plume of the predetonator is shown in Fig. 34.

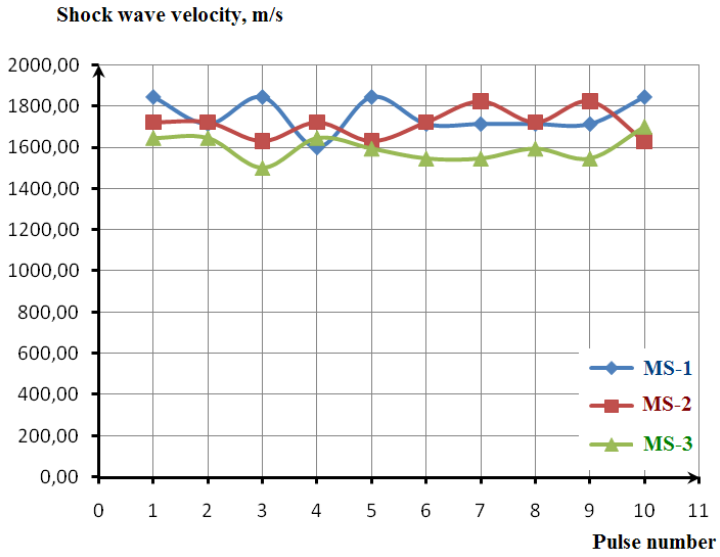

Figure 33: Measured shock wave velocities at three measuring segments MS-1, MS-2, and MS-3 (see Fig. 32) in 10 successive pulses.

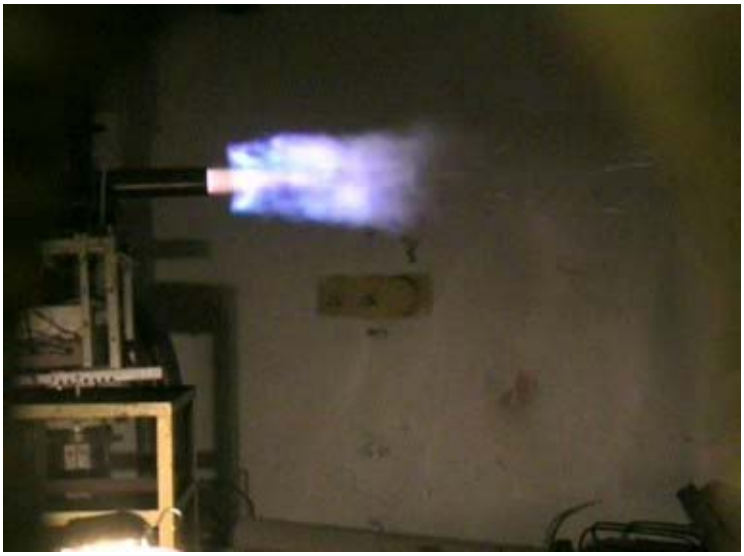

Figure 34: The plume of the predetonator operating on aviation kerosene – air mixture.

9.0 CONCLUDING REMARKS

The material discussed above indicates that there are no fundamental constrains in applying repeatedly propagating confined detonations for producing thrust. The thermodynamic evaluation of the detonation cycle in comparison with constant-pressure and constant-volume combustion cycles for propane-fueled air-breathing engines shows that thermodynamic efficiency of pulse detonation thrusters is considerably higher than that of other conventional thrusters based on combustion.

When comparing the predicted performance of the idealized PDE operating on direct detonation initiation with the performances of the propane-fueled PDEs operating on DDT at both zero flight speed and Mach 3.0 flight conditions, the DDT was shown to be a feasible approach for practical PDEs. Thus, the fuel-based specific impulse for the propane-fueled air-breathing PDE at Mach 3.0 flight conditions was estimated as $I_{sp} \approx 1550 \pm 100$ s, which is higher than the specific impulse characteristic for hydrocarbon-fueled ramjets. The DDT run-up distance and time in such conditions were shown to be so short that the engine integrating the supersonic intake, detonation chamber, bypass channel, valve distribution system, and supersonic nozzle could be quite compact with the total length as short as about 1.8 m and could operate at the altitude of 9.3 km with positive thrust at a frequency of 100 Hz and very low detonation ignition energy on the order of 1 mJ.

The possibility of obtaining a repeatable DDT in hydrocarbon fuel (aviation kerosene) – air mixture with such short run-up distances and times has been experimentally substantiated at the SICP. Several engine designs have been suggested and PDE demonstrators fabricated and tested. It has been proved experimentally that DDT in heterogeneous aviation kerosene – air mixture at atmospheric initial pressure can be repeatedly obtained at run-up distances and times shorter than 2 m and 5–7 ms, respectively, whereas the ignition energy can be as low as 0.1 J. These findings indicate that at zero flight speed conditions, a kerosene-fueled PDE operating on DDT can be fired at frequencies up to 50–60 Hz provided it is equipped with a starting device for air supply (e.g., fan, compressor, pressurized air bottle, etc.). At flight conditions, ram compression of approach stream air in the engine intake will facilitate filling and purging processes in the detonation chamber as well as decrease the DDT run-up distance and time (due to elevated mixture density), thus increasing the maximum PDE operation frequency.

Thus, with the PDE technology air-breathing propulsion seems to receive a chance of getting a long-expected breakthrough in efficiency, and, as a consequence, in increased range, payloads, etc.

10.0 ACKNOWLEDGMENTS

Valuable contribution of Dr. Aksenov V.S., Prof. Basevich V.Ya., Dr. Belyaev A.A., and MSc. Ivanov V.S. to this work is gratefully acknowledged. This work was supported by the Federal special purpose program “Scientific and teaching human resources of innovative Russia” for 2009–2013 within State contract # П502, Federal special purpose program “Research and development in priority directions of technological complex of Russia” (State contracr #02.516.12.6026), and Russian Foundation for Basic research (grant #08-08-00068).

11.0 REFERENCES

[1] Zel’dovich Ya. B. *J. of Technical Physics* 1940, Vol. 10, No. 17, pp. 1455–1461.

[2] Heiser W. H. and Pratt D. T. *Propulsion and Power*, 2001, Vol. 18, No. 1.

[3] Povinelli L. A. and Yungster S. Airbreathing Pulse Detonation Engine Performance, 2002, NASA/TM-2002-211575.

[4] Frolov S.M., Barykin A.E., Borisov A.A. Thermodynamic Cycle with Detonative Fuel Combustion. *Rus. J. Chemical Physics*, 2004, Vol. 23, No. 3, pp. 17–25.

[5] Bussing T. R. A. and Pappas G. Pulse Detonation Engine Theory and Concepts. In: *Developments in High-Speed-Vehicle Propulsion Systems*, *Progress in Astronautics and Aeronautics*, No. 165, AIAA, 1996, pp. 421-472.

[6] Ziton R. and Desbordes D. Propulsive Performance of Pulsed Detonations. *Combustion Science and Technology*, 1999, Vol. 144, pp. 93-114.

[7] Kailasanath K. Review of Propulsion Applications of Detonation Waves. *AIAA Journal*, 2000, Vol. 38, No. 9, pp. 1698–1708.

[8] Kailasanath K. Recent Developments in the Research on Pulse Detonation Engines. *AIAA Journal*, 2003, Vol. 41, No. 2.

[9] Roy G. D., Frolov S. M., Borisov A. A., and Netzer D.W. Pulse Detonation Propulsion: Challenges, Current Status, and Future Perspective. *Progress Energy and Combustion Science*, 2004, Vol. 30, No. 6, pp. 545–672.

[10] Kailasanath K. Research on Pulse Detonation Combustion Systems – A Status Report. *47th AIAA Aerospace Sciences Meeting*, AIAA, Orlando, FL, 2009-631, 2009.

[11] Frolov S.M. and Ivanov V.S. Combined Flame Tracking – Particle Method for Numerical Simulation of Deflagration-to-Detonation Transition. In: *Deflagrative and Detoantive Combustion*. Ed. by G. Roy and S. Frolov, Moscow, Torus Press, 2010, pp. 133-156.

[12] Canteins G., Franzetti F., Zitoun R., Desbordes D., Daniau E. PDE – Possible Ways for Specific Impulse Improvement. In: *Confined Detonations and Pusle Detonation Engines*. Ed. by G. Roy, S. Frolov, R. Santoro, and S. Tsyganov. Moscow, TORUS PRESS, 2003, pp. 177-190.

[13] Kailasanath K. On the Performance of Pulse Detonation Engines. In: *Confined Detonations and Pusle Detonation Engines*. Ed. by G. Roy, S. Frolov, R. Santoro, and S. Tsyganov. Moscow, TORUS PRESS, 2003, pp. 191-202.

[14] Kailasanath K. On the Performance of Pulse Detonation Engines. In: *Advances in Confined Detonations*. Ed. by G. Roy, S. Frolov, R. Santoro, and S. Tsyganov. Moscow, TORUS PRESS, 2002, pp. 207-212.

[15] Baker W.E., Cox P.A., Westine P.S., Kulesz J.J., Strehlow R.A. *Explosion Hazards and Evaluation*. Elsevier, Amsterdam-Oxford-N.Y., 1983.

[16] Veyssiere B., Kerampran S., Proust C., and Gilles S. Effect of Tube Length on Flame Acceleration and DDT in Tubes of Constant Cross Section. *Proceedings of the 19th ICDERS*, 2003, Hakone, Japan, Paper#154.

[17] Santoro R. J., Lee S.-Y., Conrad C., Brumberg J., Saretto S., Lecat P., Pal S., and Woodward R. D. Deflagration-to-Detonation Transition Studies for Multicycle PDE Applications. *Advances in Confined Detonations,* edited by G. Roy, S. Frolov, R. Santoro, and S. Tsyganov, Torus Press, Moscow, 2002, pp. 243–249.

[18] Lee S.-Y., Watts J., Saretto S., Pal S., Conrad C., Woodward R. D., and Santoro R. J. *Journal of Propulsion and Power*, 2004, Vol. 20, No. 6, pp. 1026-1036.

[19] Kerampran S., Desbordes D., and Veyssiere B. Influence of the Pressure Waves Generated at the Initial Stage of Flame Propagation on the DDT Process in Smooth Tubes. In: *Confined detonations and pulse detonation engines.* Eds. G. Roy, S. Frolov, R. Santoro, S. Tsyganov. Moscow: TORUS PRESS, 2003, pp. 3-16.

[20] Ciccarelli G., Fowler C. J., Bardon M. Effects of Obstacle Size and Spacing on the Initial Stage of Flame Acceleration in an Obstacle Laden Tube. *Proc. 19th ICDERS*, 2003.

[21] Frolov S. M. Liquid-Fueled Air-Breathing Pulse Detonation Engine Demonstrator: Operation Principles and Performance. *J. Propulsion and Power*, 2006, No. 6, pp. 1162-1169.

[22] Frolov S. M. Fast Deflagration-to-Detonation Transition. *Russian Journal of Physical Chemistry B*, 2008, Vol. 2, No. 3, pp. 442-455.

[23] Frolov S. M. and Aksenov V. S. Initiation of Gas Detonation in a Tube with a Shaped Obstacle. *Doklady Physical Chemistry*, 2009, Vol. 427, Part 1, pp. 129–132.

[24] Oppenheim A. K. *Introduction to Gasdynamics of Explosions*, Springer, Wien, 1972.